Subaqueous Moraine Building and Implications for Frontal Ablation Processes

by

Adam Scott Lucas

A thesis accepted and approved in partial fulfillment of the

requirements for the degree of

Master of Science

In Earth Sciences

Thesis Committee:

David Sutherland, Chair

John Christian, Member

Alan Rempel, Member

University of Oregon

Spring 2026

© 2026 Adam Scott Lucas

THESIS ABSTRACT

Adam Scott Lucas

Master of Science in Earth Sciences

Title: Subaqueous Moraine Building and Implications for Frontal Ablation Processes

Subaqueous moraine building is critical for tidewater glacier terminus stability, e.g., the growth and advancement of a morainal bank can stabilize the terminus of a tidewater glacier despite regional climate warming. However, our understanding of the rates of moraine building during different phases of glacier retreat or advance are limited by the lack of near terminus observations. Here, we provide novel observations of rapid vertical morainal bank growth from 2016 to 2025 at a tidewater glacier in Southeast Alaska. We compare sediment accumulation rates with changes in glacier dynamics to explore the processes that transport and deposit sediment and the associated changes in glacier flow. We find that moraine shoaling rates peak at 4-10 m yr^{-1} in 2016-2018 and increase linearly to 15-20 m yr^{-1} during 2018-2025. Subaqueous terminus area decreases by 3.2% per year from 2018 to 2023, over twice as fast as previously estimated for 1999 to 2016. Near-terminus glacier velocities decelerated by 72 m yr^{-2} during 2017 to 2025 compared to 38 m yr^{-2} during 2000 to 2015. Glacier elevation increases by 36-48 m during the rapid 2018-2025 moraine buildup. Overall, we find a dependence of tidewater glacier dynamics and frontal ablation on sediment output through the rapid and nonlinear shoaling of a subaqueous morainal bank. Despite the importance of changing subaqueous topography, many predictions of glacier evolution and sea level rise do not incorporate these processes.

ACKNOWLEDGMENTS

I wish to express my appreciation for Dave Sutherland, who has provided the guidance, support, resources, and skills needed for this project to be successful. I have grown to be an independent, inquisitive, and confident scientist under Dave's mentorship. I will miss the Oceans & Ice lab, and our many discussions about glaciology and oceanography. Many collaborators have supported this project, including but not limited to Jason Amundson, Jonathan Nash, Jesse Cusack, Trevor Harrison, Nicole Abib, their students, and many, many others. This work would not have been possible without their feedback, recommendations, and scientific discussions. I also want to thank my committee members, Alan Rempel and John Christian for their feedback and discussions. I have been fortunate enough to go into the field on a research cruise at Xeitl Sit', Alaska, and Shakes Lake, Alaska, install weather stations at Hayden Glacier, collect seismometers at Mt. Rainier, learn about machine learning in the wilderness of southwestern Montana, travel to workshops and conferences in New Hampshire, Washington, DC and New Orleans. Thank you to all that have supported these inspiring experiences.

I would also like to thank the 2024 Earth Sciences graduate student cohort for all of the wonderful friendships and experiences. When I first moved to Eugene, I did not expect to make so many friends so quickly. I will miss our adventures in the Cascades, the Oregon Coast, and late nights in Eugene. I would like to express my appreciation to Thays, Mom, Dad, Lauren, and Scott, for the encouragement and motivation from 2,700 miles away. Thays, our adventures in the Northwest and Southeast are what made the past two years special, and I am excited for many more wherever the future takes us.

Lastly, this work is financially supported by funding from the National Science Foundation and the University of Oregon Earth Sciences Department.

DEDICATION

This thesis is dedicated to Jackson. Thank you for all the wonderful memories.

TABLE OF CONTENTS

Chapter	Page
I. INTRODUCTION	9
Background	9
Physical Setting: Xeitl Sit’	12
II. METHODS	16
Bathymetry Surveys	16
Glaciological Variables	17
III. RESULTS	19
Moraine Morphology and Sediment Accumulation	19
Glacier Dynamics and Subglacial Discharge	25
IV. DISCUSSION	26
Accumulation in other Systems	26
Tidewater Glacier Cycle	28
Sediment Output	31
Importance for Ice Sheet and Ocean Modeling	32
V. CONCLUSION	34

Chapter Page

APPENDICES 35

A. SUBGLACIAL DISCHARGE MODELING 35

B. SUPPLEMENTAL FIGURES 36

REFERENCES CITED 42

LIST OF FIGURES

Figure Page

1. Schematic of moraine building processes 11

2. Location of Xeitl Sit' 13

3. Glacier terminus position, velocity, and elevation changes from 1990 to 2025 14

4. Hillshaded and gridded bathymetry. 20

5. Centerline fjord elevation and slope 21

6. Gridded sediment accumulation rates 23

7. Centerline sediment accumulation rates 24

CHAPTER I

INTRODUCTION

1.1 Background

Tidewater glaciers terminate in the ocean, losing mass at their terminus through submarine melting and iceberg calving (combined, these two processes constitute "frontal ablation"). Topography of the seafloor exerts control over frontal ablation, and therefore the glacier's terminus position. Moraines, also called sills and morainal bank complexes, are topographic high points within a fjord produced by deposition of glaciogenic sediment. Moraines can act as a barrier to warm ocean water, reducing the subaqueous terminus area available for submarine melting (Hager et al., 2022; Straneo & Cenedese, 2015). Moraines can also stabilize the glacier terminus by exerting back stress on the glacier, slowing advance and thickening the glacier (Amundson, 2016; E. Fischer & Aschwanden, 2024; M. P. Fischer & Powell, 1998). Morainal bank development drives cyclic tidewater glacier advance and retreat in a process termed the tidewater glacier cycle (TGC) (Brinkerhoff et al., 2017; Meier & Post, 1987; Post et al., 2011). In the classic TGC, relatively slow ice advance is driven by a reduction in ice discharge into the fjord by a growing morainal bank. Rapid glacier retreat occurs when a climate-driven perturbation to the glacier's terminus position causes retreat into deeper water; increasing ice discharge into the ocean causes unstable retreat as water depth increases up-fjord.

Glacier, fluvial, and oceanographic processes erode and transport sediment to create morainal bank complexes. Slip velocity at the glacier's bed is a primary control on the erosion of sediment, where faster glacier slip speed erodes more sediment (Alley et al., 2019; Cook et al., 2020; Herman et al., 2015, 2021). Temperate maritime Alaskan glaciers have high surface velocities, high surface melt, and wet, warm basal conditions, allowing for a large percentage of

terminus surface velocity to be attributable to basal slip. Substrate lithology affects erosion rates under glaciers as well, with unconsolidated sediment and faulted and jointed bedrock eroding faster than crystalline bedrock (Dühnforth et al., 2010; Hooyer et al., 2012; Krabbendam & Glasser, 2011; Norris et al., 2025). Sediment is transported to the glacier terminus by meltwater draining to the bed through crevasses and moulins, where it travels through subglacial till and channels eroded into the ice and bed (Swift et al., 2005). Estimates of glacial erosion are highest in Alaska, ranging from 10-100 mm yr^{-1}, owing to the temperate climate and dynamic glacier systems that erode large amounts of sediment (Hallet et al., 1996; Koppes et al., 2015).

Fresh meltwater is exported to the ocean where it rises as a plume into the relatively warm and saline ocean water (Straneo and Cenedese 2015; Hewitt, 2020). Discharge plumes carry suspended subglacial sediment down-fjord and particles settle out based on grain size (Fig. 1; Cowan & Powell, 1991; Mugford & Dowdeswell, 2011). Gravity currents transport previously deposited material down the slope of a morainal bank complex, filling the basin and diffusing the slopes of the moraine (Fig. 1; Boldt Love et al., 2016; Brinkerhoff et al., 2017; Pope et al., 2019). Glaciofluvial bedload dumping and hillslope mass movements have been observed to contribute the most volume gain to morainal bank complexes at several Alaskan tidewater glaciers (Hunter et al., 1996). Other processes that carry sediment, such as iceberg rafting, basal freeze-on, mechanical deformation, and supraglacial and englacial transport, contribute a small amount of moraine building at these glaciers. However, these processes are spatially variable; recent studies find that iceberg rafted debris contributes up to one third of the sediment budget of Greenlandic outlet glaciers (Pierce et al., 2026).

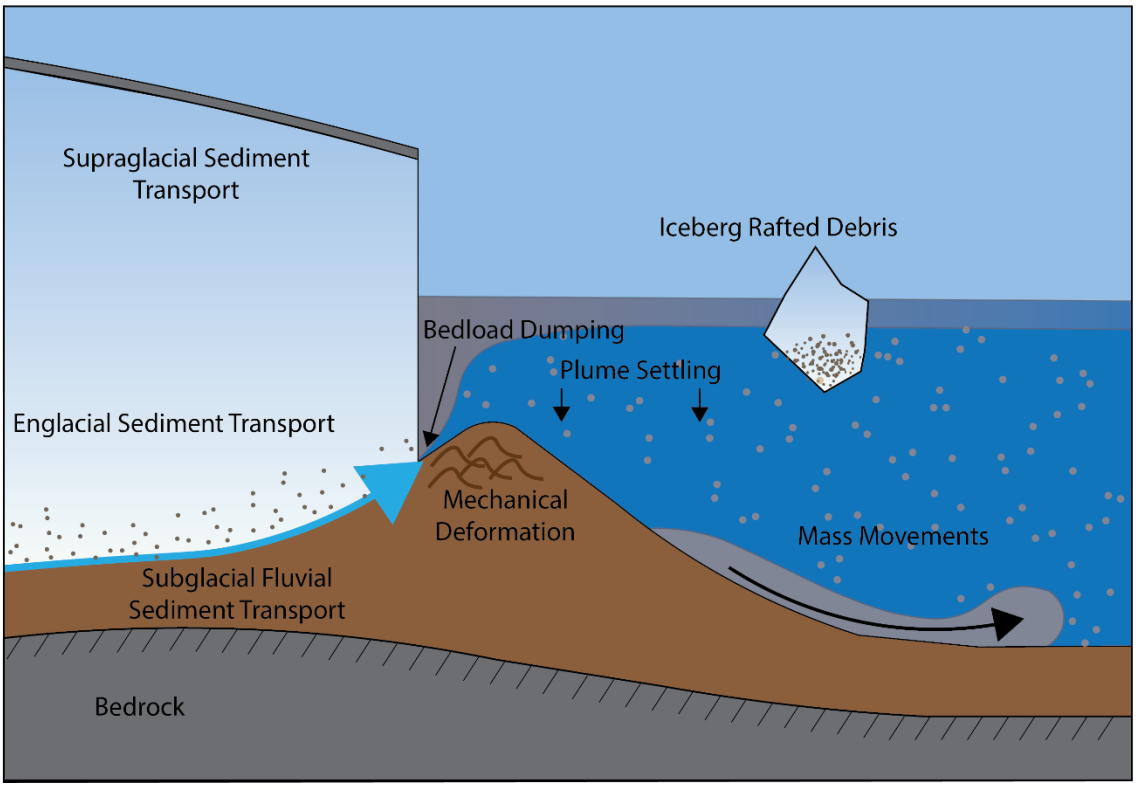


Figure 1. Schematic of moraine building processes that are important to moraine building in a temperate Alaskan setting. Supraglacial, englacial, and subglacial transport and bed deformation brings sediment to the terminus. Dumping of fluvially transported bedload, suspended sediment settlement, and transport of iceberg rafted debris are depositional processes. Mass movements remove material from the moraine. Figure is modified from Hunter et al., 1996.

Sonar bathymetry collected in 1999, 2016, 2017, and 2018 in Xeitl Geeyí (LeConte Bay), AK, show the buildup of a moraine and infilling of a basin during the stillstand and short retreat of Xeitl Sit' (LeConte Glacier) (Eidam et al., 2020). Since 2018, Xeitl Sit' has readvanced to its previous stillstand position. Few observational studies attempt to quantify the change in glacier dynamics during the buildup of a morainal bank. We use new sonar bathymetry of Xeitl Geeyí collected in 2023, 2024, and 2025, to explore morainal bank growth. In this paper, we present novel observations of vertical morainal bank shoaling and down-fjord progradation. We combine observations of morainal bank growth with near-terminus glacier dynamics to explore how morainal bank growth drives the glacier advance phase of the TGC.

1.2. Physical Setting: Xeitl Sit'

Xeitl Sit' (LeConte Glacier), a 480 km^2 glacier located in Southeast Alaska drains from the 5800 km^2 Stikine Icefield and is the southernmost tidewater glacier in the Northern hemisphere (Fig. 2; Melkonian et al., 2016). Xeitl Sit' has a complex history of retreat and stabilization at morainal bank complexes (Eidam et al., 2020; Motyka et al., 1998, 2003; O'Neel et al., 2003). The glacier's furthest known extent is marked by a Little Ice Age moraine at the entrance to Xeitl Geeyí. The glacier terminus stabilized at Morainal Bank complex 1 (MB1) from 1962 to 1994 (Figs 3, 4), after which it underwent a rapid 2 km retreat from 1994-1999 and stabilized at a constricted bend in the fjord, where it built morainal bank complex 2 (MB2). The glacier stabilized on MB2 from 1999-2016, after which it underwent a ~0.5 km retreat and a slow advance back to the MB2, at which it has restabilized (Figs 3, 4). Terminus positions vary seasonally, with winter advances and summer retreats on the order of 50-200 m (Fig. 3). During the glacier's retreat from MB2, the newly uncovered basin filled with 6.6×10^5 m^3 of sediment, raising the seafloor by 40 m (Eidam et al., 2020).

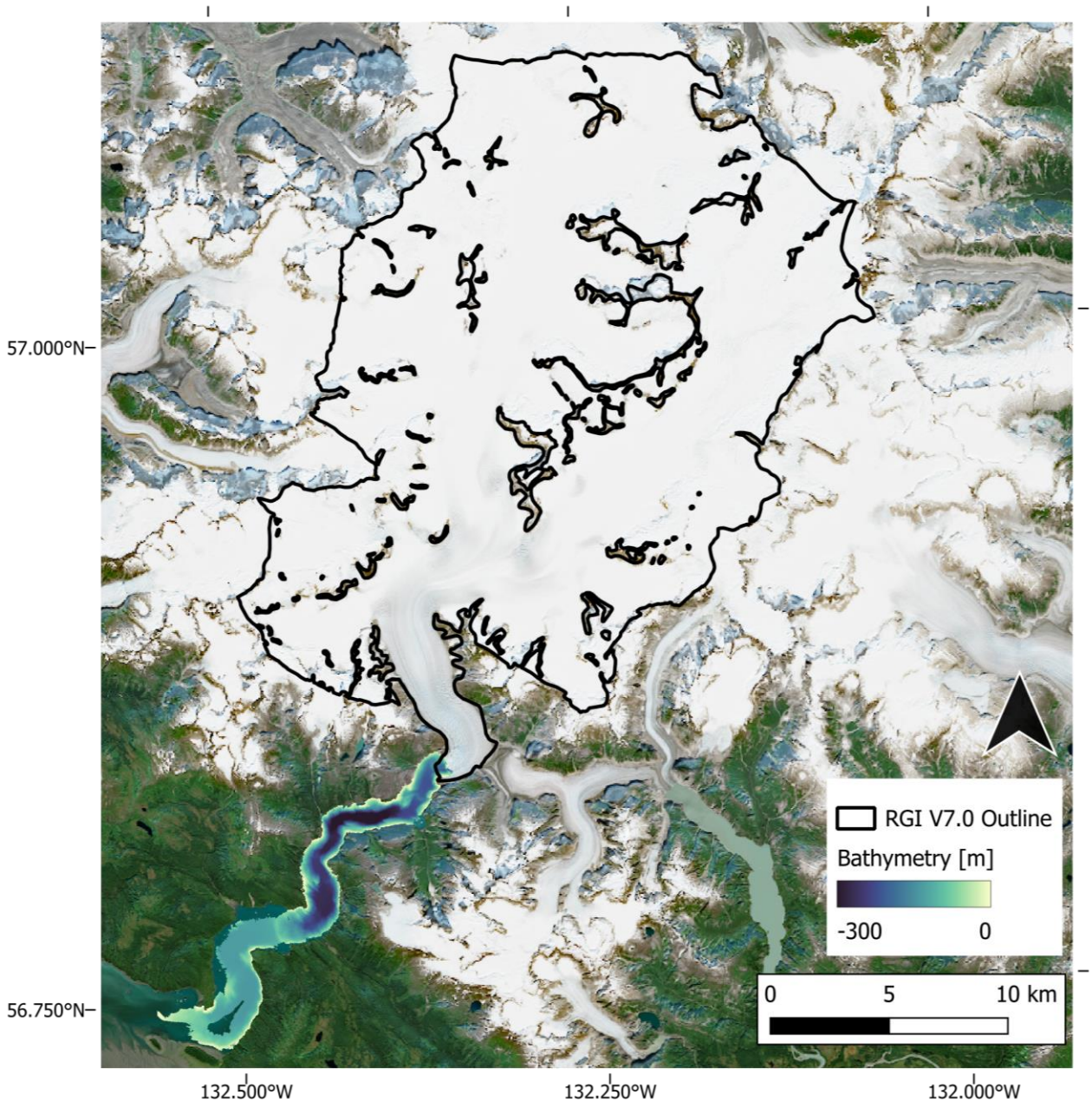


Figure 2. Location of Xeitl Sit'. RGI v7.0 outline of Xeitl Sit' and August 2016 bathymetry covering the entire fjord.

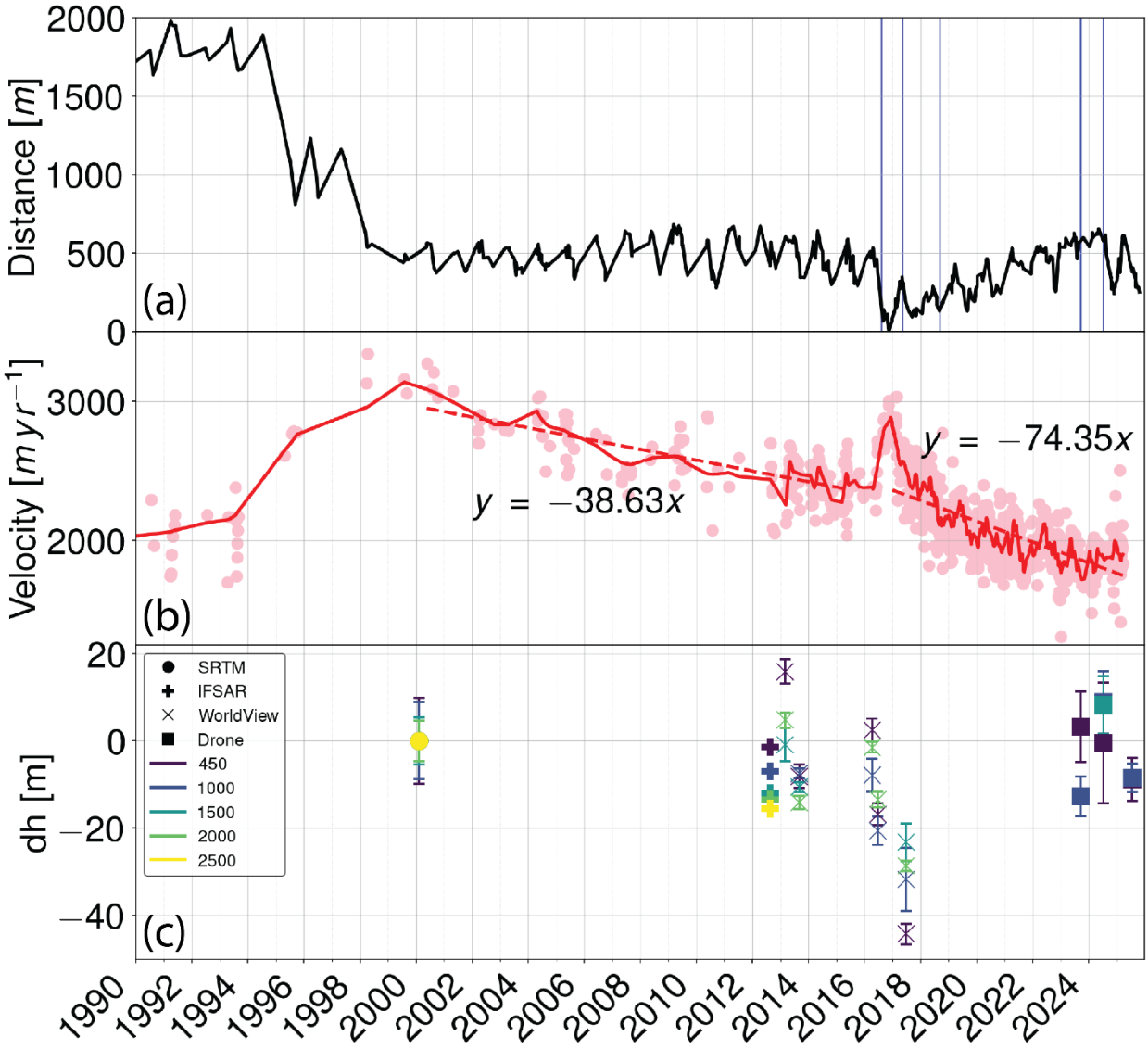


Figure 3. Glacier terminus position, velocity, and elevation changes from 1990 to 2025. (a) Glacier terminus position along the middle centerline in Figure 4d, (b) ITS_LIVE velocities at a point ~3 km up glacier from the 2023 terminus (56.85561, -132.34634), and (c) glacier elevation change from the Shuttle Radar Topography Mission (SRTM) elevation at 450, 1000, 1500, 2000, and 2500 m up-glacier from the 2023 terminus position. Vertical blue shaded regions correspond to field seasons. The solid red line in (b) is a LOWESS regression of the raw velocity data.

Xeitl Sit' is underlain by a granodiorite batholith and strong, erosion-resistant tonalite (Brew & Friedman, 2000). Velocities measured at the glacier's terminus, where plug flow is assumed, are high at 15-25 m d^{-1} (Abib et al., 2023; Sutherland et al., 2019). Large amounts of meltwater discharge at Xeitl Sit' are predicted from surface mass balance models (~250 m^3 s^{-1}) (Amundson et al., 2020; Jackson et al., 2020, 2022; Sutherland et al., 2019). Therefore, sediment erosion at Xeitl Sit' is limited by strong lithology but increased through high slip velocity and availability of subglacial meltwater to transport material. Mean catchment erosion rates are relatively low at 1.4-4.0 mm yr^{-1}, potentially due to the erosion resistant tonalite batholith underneath the glacier (Eidam et al., 2020; Hunter (unpublished data)).

CHAPTER II

METHODS

2.1 Bathymetry Surveys

Multibeam sonar mounted on watercraft collected bathymetry data in Xeitl Geeyí. In August 1999 and September 2000 sonar data were collected with a Furuno 528L fathometer and Trimble Pro XRS GPS Receiver and data logger (Hunter and Motyka, unpublished data). In August 2016 data were collected using a Reson SeaBat 7111 multibeam echosounder and an Applanix POS/MV 320 WaveMaster, and in May 2017 and September 2018 using a Reson SeaBat T50-P multibeam system. The 1999/2000, 2016, 2017, 2018 sonar data collection and processing methods are described in detail in Abib et al., 2023, Eidam et al., 2020, and Sutherland et al., 2019.

In September 2023 and July 2024 a Norbit i80s Winghead multibeam sonar was deployed from both an autonomous Rigid-Hulled Inflatable Boat (RHIB) and manually from a small, manned watercraft. A Lowrance Elite FS-9 singlebeam echosounder was deployed from the autonomous RHIB in 2025. The multibeam sonar surveys produced a 3D point cloud covering the near terminus glacier, seafloor, and fjord sidewall morphology. Sonar scans were collected multiple times a day during each of the ~2-week cruises. Seafloor morphology was manually separated from terminus morphology by finding slope breaks at the transition from seafloor to glacier ice using the point cloud editing software CloudCompare. All point clouds collected within a field season are stacked and gridded at a 2 m resolution using the sonar processing software MBSystem (Caress & Chayes, 1996). A spline interpolation filled gaps of 10 grid cells or less. Bathymetric grids are exported to Python for further geospatial analysis. Uncertainty is measured by estimating the average change in elevation over an area of stable bedrock, where elevation should be unchanging (Fig. A-1). These uncertainties are -0.85, 0.53, 0.34, -2.47, and -1.56 m for

1999-2016, 2016-2017, 2017-2018, 2018-2023, and 2023-2024 respectively. To be conservative, the highest elevation error determines the uncertainty for the entire bathymetry dataset, which is ±2.5 m (Eidam et al., 2020; Schimel et al., 2015). Gridded linear sediment accumulation rates are calculated by dividing elevation differences by the difference in time between surveys.

2.2. Glaciological Variables

Terminus positions were manually traced from Landsat and Sentinel satellite imagery using the GEEDIT software, providing multi-decadal observations of terminus fluctuations (Lea, 2018). Terminus positions with a higher spatial resolution (~1 m scale) were traced in QGIS on drone-based orthomosaics of the glacier's terminus created using the structure-from-motion photogrammetry software Agisoft Metashape.

Glacier velocities were extracted from the ITS_LIVE velocity dataset (Gardner et al., 2022), which uses image pair feature tracking of Landsat and Sentinel images to create glacier velocity maps (Gardner et al., 2018). Because of sparse velocity data near the glacier's terminus, we extract the glacier velocity at a point ~3 km upstream of the 2023 terminus (56.85561, -132.34634). ITS_LIVE velocities are smoothed using a LOWESS filter (LOcally WEighted Scatterplot Smoothing) (Derkacheva et al., 2020).

Glacier elevation changes are explored using satellite- and drone-based Digital Elevation Models (DEMs). Drone DEMs of the terminus were created using top-down photographs of the glacier input into Agisoft Metashape. DEMs were produced at 0.2-1 m spatial resolution and upscaled to 1 m resolution for comparison. Satellite data sources include the Shuttle Radar Topography Mission (SRTM) DEM on February 11, 2000 (Farr et al., 2007), Alaska Interferometric Synthetic Aperture Radar (IfSAR) DEM on August 14, 2012

(https://www.usgs.gov/centers/eros/science/usgs-eros-archive-digital-elevation-interferometric-synthetic-aperture-radar), and Worldview DEMS on March 7 and September 6, 2013, April 10 and June 20, 2016, and June 23, 2017 accessed through the Polar Geospatial Center (Porter et al., 2018). All DEMs were coregistered to the 2018 IfSAR DEM using the xDEM Python module (xdem contributors, 2026) to apply a vertical shift and the coregisteration method described in Nuth & Kääb, 2011.

We model subglacial discharge rates using an Enhanced Temperature Index melt model coupled to an accumulation model and a linear reservoir discharge routing model (Hock, 1999; Hock & Noetzli, 1997), described in detail in Appendix A. We employ a similar methodology to that of previous studies of Xeitl Sit' (Amundson et al., 2020; Jackson et al., 2022; Sutherland et al., 2019). Summer melt seasons were manually delineated when discharge steeply increases during the spring and decreases during the fall. We then average discharge values over the time-variable summer melt season to compare with sediment accumulation rates.

CHAPTER III

RESULTS

3.1 Moraine Morphology and Sediment Accumulation

Moraine morphology changes were investigated by comparing gridded bathymetry over multiple years. MB2 is shown as an arcuate elevated ridge near the glacier terminus in the same shape as the terminus (Fig. 4). MB2 is at 160 m depth from 2016-2018 and shallows to 90-120 m depth in 2023-2025. In 2016-2018, the glacier retreated entirely off MB2, revealing the backside of the moraine. In 2023 and 2024, only the glacier-distal slope of MB2 is visible, and the glacier had advanced to near the moraine crest. In 2025, the glacier had retreated off MB2 and a portion of the glacier-proximal slope is visible. The seafloor shoaled by 30-60 m at the crest of MB2 from 2018 to 2023 (Figs 4, 5). The glacier-distal basin shallows by ~15 m over 2018-2023. The glacier-proximal basin shallowed by ~30 m from 2018-2025. The moraine crest, or the line tracing the highest elevation of the moraine, shows little horizontal change from 2016-2023. From 2023-2024 the moraine crest moved horizontally down-fjord by ~30 m. The glacier-distal moraine slope prograde forward at the 160 m isobath by 35 m between 2023-2024 and 48 m between 2024-2025 (Fig. A-2). Slopes on the glacier-distal moraine slope are highest at 38° in 2024, 33° in 2023, and 29° in 2025, increased from 31° in 2016, 27° in 2017 and 2018 (Figs 5, A-3).

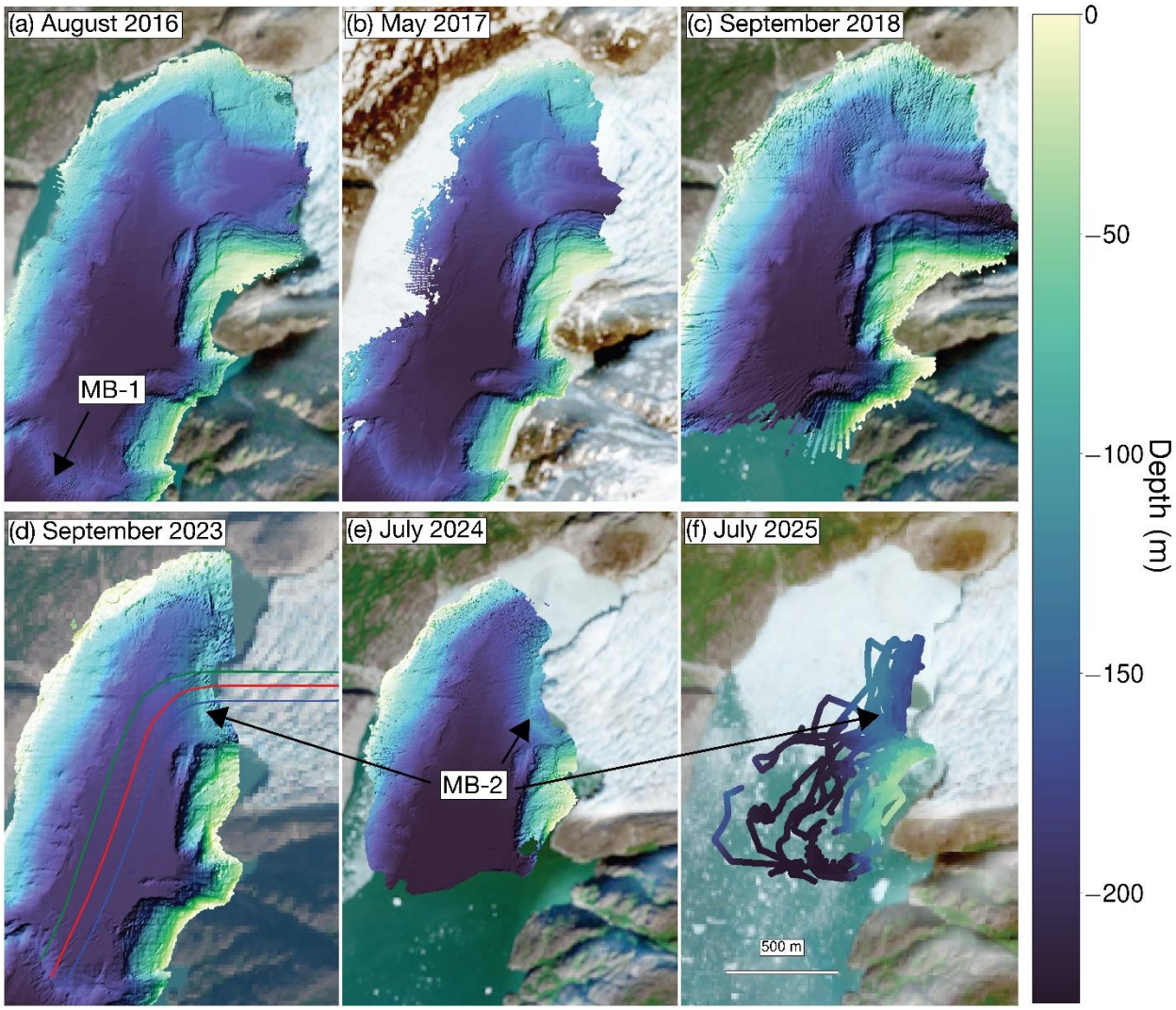


Figure 4. Hillshaded and gridded bathymetry**.** Hillshaded and gridded bathymetry in Xeitl Geeyí for (a) August 2016, (b) May 2017, (c) September 2018, (d) September 2023 and (e) July 2024, and (f) echosounder tracks for July 2025. Background imagery is from the Sentinel-2 satellite. Centerlines used to extract fjord bathymetry and sediment accumulation rates in Figure 5 and 7 are shown overlain on 2023 bathymetry (d). MB-2 is only indicated on d-f for clarity but is visible on a-c as well.

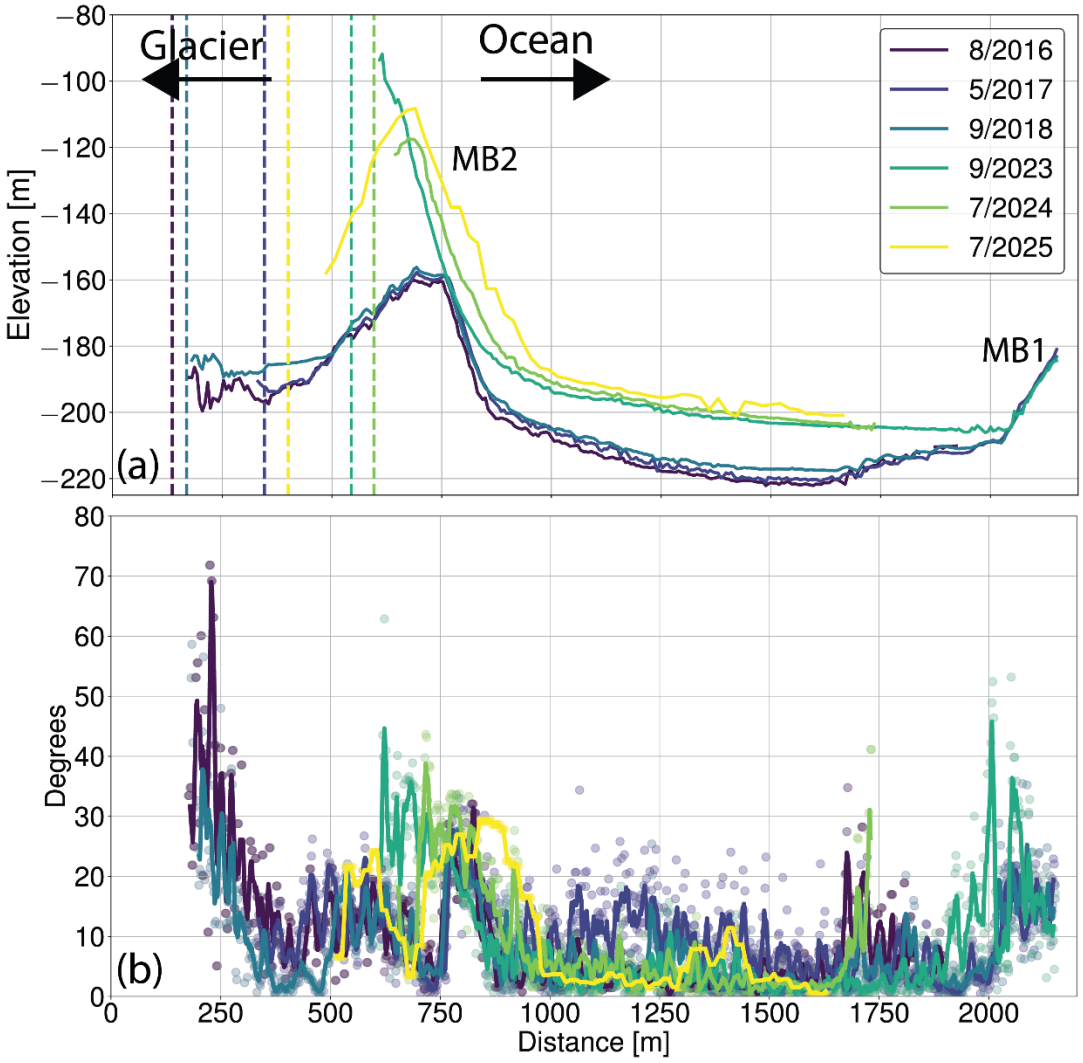


Figure 5. Centerline fjord elevation and slope. (a) Bathymetry along the middle centerline in Figure 4.d. in Xeitl Geeyí. Dashed lines show the terminus position corresponding to the bathymetry of the same color. (b) Absolute value of fjord seafloor slopes along the middle centerline in Figure 4.d. smoothed with a 3-point moving average.

Maximum sediment accumulation rates are highest directly in front of the glacier (Figs 6, 7). Sediment accumulation rates peak behind the moraine in 2016-2018, infilling the glacier-proximal basin (Figs 6, 7). In 2018-2023, maximum sediment accumulation rates occur on the moraine crest, vertically shoaling it. In 2023-2025 the maximum sediment accumulation rate was located on the

glacier-distal slope, advancing the moraine horizontally down-fjord but contributing little to vertical growth (Figs 6, 7). Linear sediment accumulation rates along the middle centerline transect peak at 7, 10, 6, 15, 16, and 20 m yr^{-1} for 1999/2000-2016, 2016-2017, 2017-2018, 2018-2023, 2023-2024, and 2024-2025, respectively, and all decrease to 1-4 m yr^{-1} at 1 km down the centerline (Fig. 7). Two distinct periods emerge where maximum sediment accumulation rates are relatively low before 2018 (6-10 m yr^{-1}) and relatively high after 2018 (15-20 m yr^{-1}). Within the downstream distal basin, accumulation rates reach 1.8, 2.6, 1.5, 2.5, 2.4, and 3.9 m yr^{-1} for 1999/2000-2016, 2016-2017, 2017-2018, 2018-2023, 2023-2024, and 2024-2025 respectively (Fig. A-4). Along the southern centerline transect, accumulation rates reach ~20 m yr^{-1} during 2017-2018 where basin infill occurs (Fig. 7). Accumulation rates on the glacier-proximal moraine slope are negative in 2023-2024 at -20 m yr^{-1}. Sediment erosion on the back side of the moraine and accumulation on the front side of the moraine indicates that the moraine crest is advancing down-fjord. This could be possible in other years but not shown in the bathymetry, as sonar coverage directly at the grounding line is sparse. The moraine crest in 2024 is ~30 m down-fjord from the 2023 moraine crest and is deepened by 20 m.

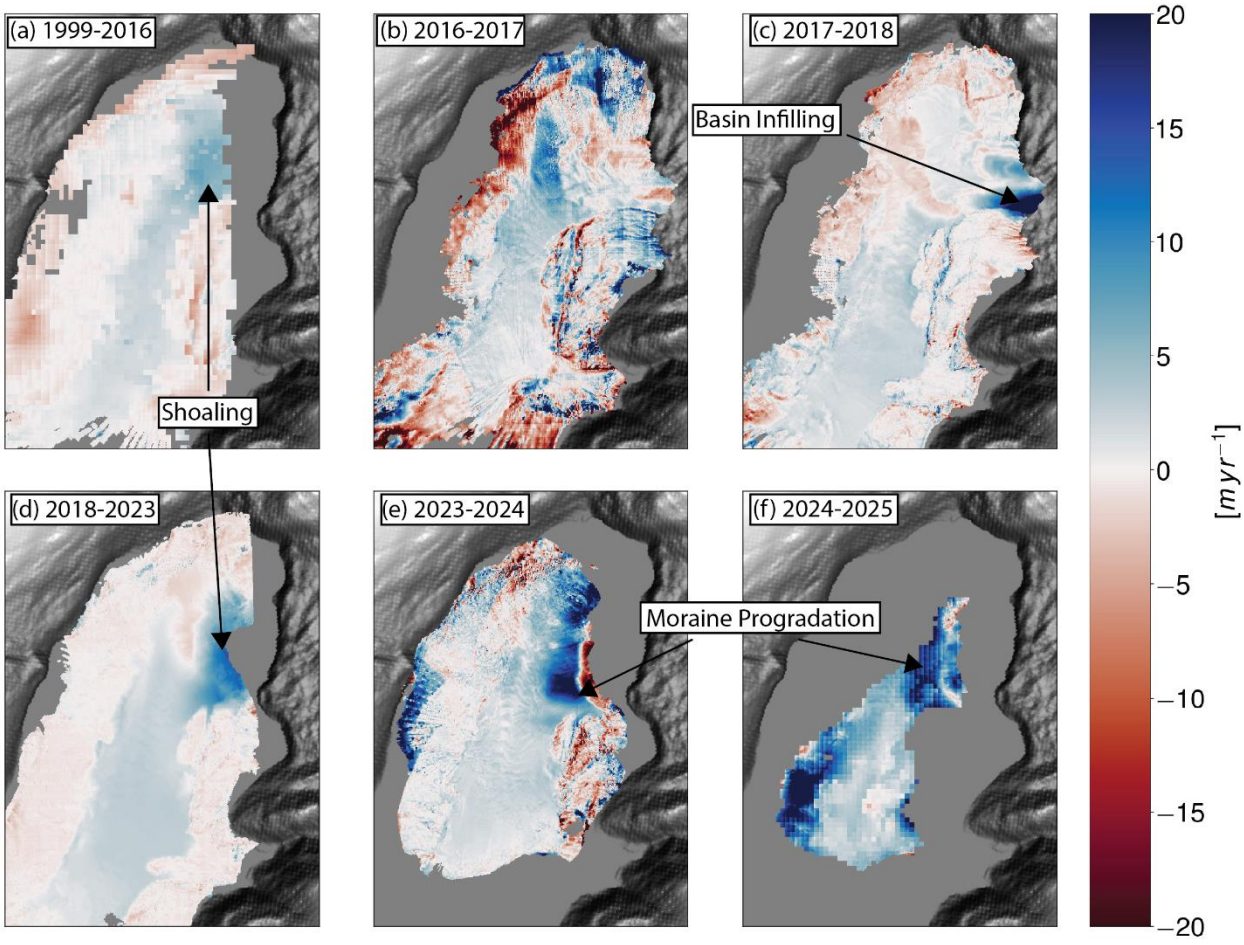


Figure 6. Gridded sediment accumulation rates. Gridded sediment accumulation rates within Xeitl Geeyí calculated between (a) 1999/2000 and August 2016, (b) August 2016 and May 2017, (c) May 2017 and September 2018, (d) September 2018 and September 2023, (e) September 2023 and July 2024, and (f) July 2024 and July 2025.

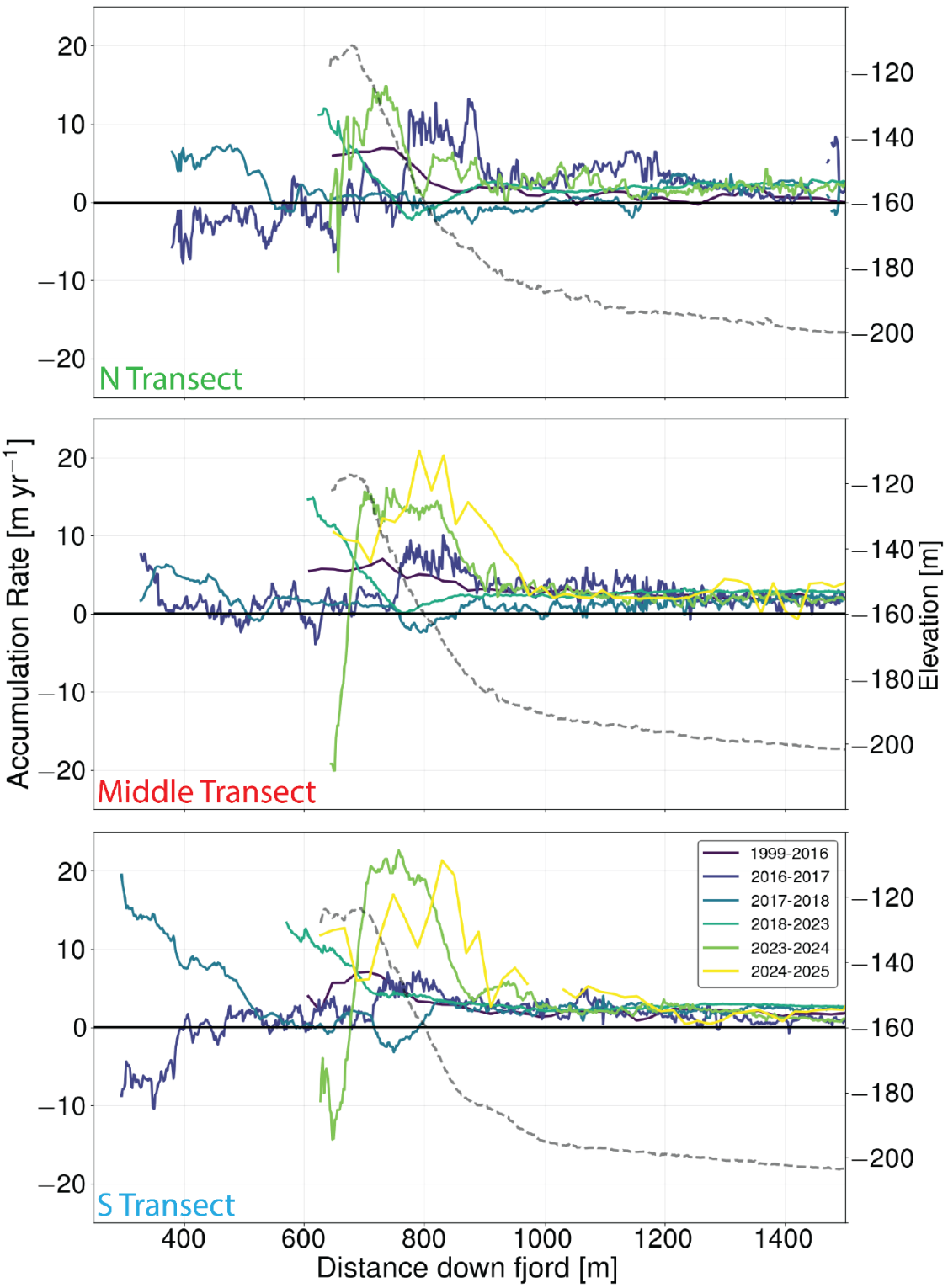


Figure 7. Centerline sediment accumulation rates. Linear sediment accumulation rates (elevation change rates) along three centerline transects shown in Figure 4.d. Grey dashed line is the 2024 seafloor elevation along the same transects.

3.2 Glacier Dynamics and Subglacial Discharge

Glacier velocities decrease steadily during the stillstand and increase during retreats. The sharp increase in average annual velocity of 2500 m yr^{-1} during 2016 coincides with a retreat of ~0.5 km, and the 1000 m yr^{-1} increase from 1994 to 1998 occurs during a 1500 m retreat of the terminus from MB1 to MB2 (Fig. 3). Glacier velocities decelerate by -38 m yr^{-2} annually during the period 2000-2016 and -74 m yr^{-2} annually during the period 2017-2025 (Fig. 3).

Change in glacier elevation from the 2000 SRTM elevation at five points with increasing distance up-glacier is plotted in Figure 3c. Closest to the terminus, glacier elevation remains within ±17 m of the SRTM elevation between 2000 and 2017. During June 2017, and following the 2016 terminus retreat, glacier elevation decreases to -44 m below SRTM elevation. This trend continues with distance upstream, however, less drawdown of glacier ice occurs up-glacier. June 2017 elevation changes are at -32 m and -29 m at 1000 and 2000 m upstream of the 2023 terminus respectively. Drone-based elevations in 2023-2025 and after the readvance of the glacier return to within ±10 m of the SRTM elevation.

Variations in subglacial discharge are compared with sediment accumulation rates (Fig. A-4). No statistical association between sediment accumulation and average subglacial discharge within a melt season is found ($r^2 = 0.05$, $p = 0.72$). Average melt season subglacial discharge rates between field seasons vary between 55 and 180 $m^3\ s^{-1}$, with the highest rates between 2017 and 2018 (98 to 180 $m^3\ s^{-1}$) and the lowest rates between 2016 and 2017 (55 to 88 $m^3\ s^{-1}$) (Fig. A-5).

CHAPTER IV

DISCUSSION

Evidence of rapid vertical growth of a morainal bank corresponding with glacier deceleration and increased surface elevation is revealed through a combination of repeat bathymetric surveys and satellite data. Xeitl Sit' stabilizes at a fjord constriction from 2000-2016, at which a morainal bank is formed increasing in elevation from -270 m in 1999/2000 to -150 m in 2016 at its shallowest point. During this time period, glacier velocities steadily decrease from ~3000 m yr^{-1} to ~2500 m yr^{-1} and near-terminus glacier elevations are between 96-120 m. A relatively short but rapid retreat (0.5 km over 5 months) accelerates glacier velocity by 250 m yr^{-1} during 2016 and draws down the glacier's surface elevation by ~40 m by mid-2017. A subsequent readvance out to MB2 occurs corresponding with rapid moraine building at 15-20 m yr^{-1}, 3-4x the rate estimated between 1999 and 2018, shoaling the moraine by 30-60 m between 2018 to 2023. Glacier velocities decelerate almost twice as fast during the readvance, and pre-retreat glacier elevations are observed after readvancing. In the following discussion, we compare accumulation rates to those in other tidewater glacier systems and discuss implications for the tidewater glacier cycle and the importance of these observations for ice sheet and ocean modeling.

4.1. Accumulation in other systems

Due to the transience of morainal banks within a fjord environment, few estimates of vertical shoaling exist. Our estimates of moraine shoaling at Xeitl Sit' are 30-60 m at the moraine crest over ~5 years, ~6-12 m yr^{-1} of moraine crest elevation gain. In Alaska, the morainal bank in Disenchantment Bay (Hubbard Glacier) advances at 34.2 m yr^{-1} over 32 years, compared to 43-48 m yr^{-1} Xeitl Sit' (Goff et al., 2012). However, Goff et al., (2012) do not measure direct vertical

shoaling rates. Motyka & Truffer (2007) observe sediment accumulation rates of 4 m yr^{-1} in Disenchantment Bay directly adjacent to the glacier front, filling in a channel between the glacier and a bedrock ridge that was previously scoured by an outburst flood. At Muir Glacier, Alaska, the seafloor shoals at the grounding line from 100 m to 30 m depth from 1978 to 1991, roughly 5 m yr^{-1} of vertical growth (Hunter & Powell, 1995). Morainal bank shoaling of 1.5 m yr^{-1} was observed in the proglacial lake of Glaciar Perito Moreno, Patagonia (Minowa et al., 2026). At Johns Hopkins Glacier, Alaska, moraine shoaling was observed at 1-2 m yr^{-1} (Kaluzienski et al., 2023).

The zone of highest accumulation occurs proximally to Xeitl Sit' and decreases exponentially with distance down-fjord (Figs 6, 7). This behavior has also been observed in Glacier Bay (Cowan et al., 2010; Cowan & Powell, 1991), Disenchantment Bay (Goff et al., 2012), the Austfonna Ice Cap in Svalbard (Dowdeswell et al., 2015), and in models of plume-based sedimentation (Mugford & Dowdeswell, 2011). Cold-based Antarctic tidewater glacier systems show diffuse and spatially variable sedimentation on the order of mm yr^{-1} with no clear down-fjord gradient (Eidam et al., 2019). Polythermal glaciers in Svalbard deposit sediment at subglacial discharge outlets on the order of cm yr^{-1} to m yr^{-1}, creating grounding line fans (Kehrl et al., 2011; Trusel et al., 2010). The magnitude of distal accumulation rates at Xeitl Sit' are similar to other Alaskan glaciers, such as at Hubbard Glacier, where downstream accumulation rates are ~1 m yr^{-1} compared to Xeitl Sit's 1-4 m yr^{-1} (Goff et al., 2012). Sediment accumulation rates in Prince William Sound during the rapid retreat of Columbia Glacier are estimated to be 5 cm yr^{-1}, several orders of magnitude less than at Xeitl Sit' (Boldt Love et al., 2016). At Yahtse Glacier, sedimentation rates are ~2 m yr^{-1} at a distance of 2.5 km from the glacier's terminus (Bartholomaus

et al., 2013). Sediment accumulation at Taku Glacier are estimated to be 0.09-2.88 m yr^{-1}, eventually shoaling the moraine to the water surface (Zechmann et al., 2021).

Iceberg rafted debris (IRD) contributes ~33% of the sediment budget of Greenlandic outlet glaciers (Pierce et al., 2026) and 0.1-9% of the sediment budget for Grand Pacific and Muir glaciers in Alaska (Hunter et al., 1996). Glaciofluvial bedload dumping (coarse grained material deposited near the grounding line) was found to be 50-80% of the sediment budget at Grand Pacific and Muir glaciers (Hunter et al., 1996). We do not attempt to calculate a sediment budget based on different sources of sediment within this study; however, we find no correlation between subglacial discharge and sediment accumulation, potentially signifying that glaciofluvial sediment transport is supply-limited (i.e. sediment transport is controlled by the supply of sediment rather than the supply of meltwater).

4.2. Tidewater Glacier Cycle

Glacier advance during the TGC is facilitated by the sustained advance of a morainal bank complex that reduces ice flux into the fjord. TGC theory finds glacier advance to occur on timescales on 100s to 1000s of years (Barclay et al., 2009; Brinkerhoff et al., 2017; Motyka & Begét, 1996). Rapid retreat off of morainal banks occurs on timescales of decades (O'Neel et al., 2005). We find short retreats and advances of Xeitl Sit' occurring on timescales of less than a decade, highlighting high variability of tidewater glacier systems.

The model of Brinkerhoff et al., (2017) shows fluvial erosion of overridden sediment directly underneath the terminus and deposition in front of the terminus during the advance phase of the TGC, supported by observations of rapid fluvial erosion of overridden soft sediment (Motyka et al., 2006). Between 2023 and 2024, a negative accumulation signal is observed on the

glacier-proximal side of the morainal bank at Xeitl Sit' (Figs 6, 7). The moraine crest advances ~30 m down-fjord during this time period. The seasonal retreat of Xeitl Sit' in 2024 uncovered where overridden sediments had been eroded and remobilized while the glacier was advanced to its farthest seasonal extent. For the moraine to advance, a constant influx of sediment is required to continually over-steepen the moraine and produce mass movements that remove deposited material. For the moraine to vertically grow, sediment transport to the moraine must exceed gravity driven mass movements of material off the moraine. Alternatively, the basin in front of the moraine could be filled enough to reduce and stabilize the moraine slopes allowing for vertical moraine growth. MB2 steepened from 2018 to 2023, encouraging mass movements and a reduction of the moraine crest height (Fig. 5). Following years show morainal bank progradation rather than vertical shoaling.

Morainal bank complexes limit melting at the termini of tidewater glaciers, stabilizing the glacier and inducing advance. The glacier's subaqueous terminus exposure is reduced by 16% from September 2018 to September 2023. This represents a change of 3.2% per year, significantly more than the change calculated in Eidam et al., 2019, which found a change in terminus exposure of 22% in 17 years, or 1.3% per year. Xeitl Sit' has a mass balance of -0.93 m.w.e. a^{-1} (Berthier et al., 2018) and a high Accumulation Area Ratio (AAR; 0.81 between 2018 and 2022) (Zeller et al., 2025). Due to this large AAR, it is likely that frontal ablation drives drawdown of ice and is the largest source of ablation. Continued high sedimentation rates could cause MB2 to reach the water surface, blocking frontal ablation and causing the glacier to advance. Morainal banks that reach the water surface have been observed in Alaska, e.g., Taku and Johns Hopkins glaciers (Kaluzienski et al., 2023; Truffer et al., 2009). Despite the reduction in subaqueous terminus area and subsequent reduction in frontal ablation, recent laboratory

studies that compare sediment-laden plumes and ice melt show that subaqueous melt rates can be increased up to 60% with the presence of suspended sediment that enhances plume velocities (McConnochie & Cenedese, 2023). More work is needed to determine the importance of this process on a geophysical scale and its relative significance compared to reductions in terminus surface area.

Glacier velocity is shown to be steadily decreasing over the periods 2000-2015 and 2017-2025, during which the morainal bank is building (Fig. 3). After the 2016 retreat, velocities decrease at a faster rate than after the mid-1990s retreat (-38 m yr^{-2} during 2000-2015 and -74 m yr^{-2} during 2017-2025) and reach lower velocities than when the glacier was in the same location with a deeper moraine (2400 m yr^{-1} in 2015 and 1900 m yr^{-1} in 2025). Morainal banks apply backstress, or an up-glacier force, slowing glacier velocities. A change in the force balance occurring from increased backstress from a morainal bank causes disequilibrium in glacier flow, and a return to steady state can take years to decades (Benn & Evans, 2010; O'Neel et al., 2005). MB2 shoaled more rapidly in 2017-2025 than in 2000-2015, applying a higher backstress to the glacier and decelerating the glacier more rapidly. Force balance models of moraine backstress find higher backstress forces from higher morainal bank heights (M. P. Fischer & Powell, 1998) and glacier models that incorporate moraine backstress find decreasing ice velocity during advance onto a sill (Amundson, 2016).

The Stikine Icefield is a plateau icefield, with Xeitl Sit' having 81% of its area above the 2018-2022 average ELA at 1030 m, leaving the glacier vulnerable to large areas of ice being exposed to ablation with small climate-induced changes in ELA (RGI Consortium, 2023; Zeller et al., 2025). Future climate warming could reduce the surface mass balance enough that glacier advance does not occur despite a moraine induced reduction in frontal ablation, which has been

predicted in models of the TGC under a constant decrease in surface mass balance (Brinkerhoff et al., 2017). In addition, warm ocean temperatures that extend into the late summer and early fall could lead to larger seasonal retreats perturbing the glacier off the shallow moraine, where increased water depths can lead to rapid retreat. Intriguingly, the 2016 retreat of Xeitl Sit' occurred shortly after the 2013-2015 Northeast Pacific marine heatwave that drove sea surface temperatures ~3 °C degrees higher compared to previous years (Di Lorenzo & Mantua, 2016).

4.3. Sediment Output

Larger volumes of meltwater can carry higher sediment loads in proglacial streams (Stott & Mount, 2007). Subglacial discharge and mass accumulation rates correlate strongly at Greenlandic outlet glaciers over 1950-2009 (Andresen et al., 2024). No association between sediment accumulation rates and subglacial discharge is found at Xeitl Sit'. Instead, the increase in sediment output could be tied to changes in accessibility of till that could be readily mobilized. The short readvance could have remobilized and eroded overridden sediment deposited in the glacier-proximal basin (Eidam et al., 2020), leading to an increase in sediment accumulation by either glaciofluvial erosion or mechanical bulldozing of till. Subglacial channel location influences sediment transport, as subglacial channels may not reach adjacent sediment reservoirs (Delaney et al., 2023).

An increase in mass movements is likely with an increase in slope and subglacial transport of sediment. Models of moraine building have used a diffusion coefficient multiplied by the seabed gradient (Boldt Love et al., 2016; Brinkerhoff et al., 2017), where steeper slopes diffuse faster than shallower slopes. MB2 steepened from 27°-31° degrees in 2016-2018 to 29°-38° in 2023-2025, likely significantly increasing the influence of hillslope processes. This is higher than past

estimates of the slope of over consolidated, unsorted proglacial diamictons with slopes of 6-18° (Eidam et al., 2020; Goff et al., 2012; Hoek & Bray, 1981; Larter & Barker, 1989; Seramur et al., 1997). The concentration of sediment in subglacial discharge could drive gravity currents as high concentrations increase the density of discharge so that a gravity current forms rather than a buoyant plume. Dune-shaped bedforms are visible below the moraine in all years, potentially indicative of cyclic steps (Figs 4, 5, A-6). Cyclic steps are antidune bedforms that migrate upslope, thought to be formed from sediment-laden turbidity currents (Slootman & Cartigny, 2020). The presence of dune-shaped bedforms below MB2 could indicate gravity driven mass movements, consistent with the more diffuse slopes of MB2 in 2024 and 2025 (Fig. 5).

4.4. Importance for Ice Sheet and Ocean Modeling

Tidewater glaciers resting on retrograde bed slopes are thought to be susceptible to rapid irreversible retreat, a process that underlies Marine Ice Sheet Instability (MISI) theory (Schoof, 2007). The TGC essentially involves a similar process, but with seafloor topography that co-evolves with glacier dynamics. Sergienko et al. (2026) highlight that ice sheets are systems with intrinsic variability coupled to the rest of the Earth system. Observations of subglacial discharge, ice dynamics, sediment dynamics, and topography at Xeitl Sit' shows stochastic variability that transfers to glaciers evolution. The stillstand periods of Xeitl Sit' are punctuated by a short 0.5 retreat, with dynamical changes similar to what is expected during the retreat phase of the TGC. The readvance of the glacier places the glacier in a new equilibrium state, with lower glacier velocities than before the natural variability in the tidewater glacier system caused retreat. More work is needed for accurate glacier evolution models that consider short term variability in glacier and sediment dynamics.

Geometry (bed elevation, bed slope, ice thickness, surface elevation) is thought to be closely tied to the evolution of Greenlandic outlet glaciers with the glacier bed being of particular importance (Catania et al., 2018; E. Fischer & Aschwanden, 2024; Shionalyn et al., 2026). Sedimentation rates at Xeitl Sit' are larger than observed rates of bedrock uplift associated with deglaciation, indicating that these processes are important for understanding mass loss of ice sheets and sea level rise (Barletta et al., 2018). Coupled sedimentation and ice dynamical processes are missing from sea level rise predictions, highlighting the importance of new observations and modeling efforts (Aschwanden et al., 2021). The timescales of short advance and retreat that occur with coupled sediment and glacier dynamics are absent from many models. Xeitl Sit' is an example of a tidewater glacier that shows similar behavior to the TGC but on timescales of 1-20 years.

Glacier models directly depend on grounding line depth to estimate frontal ablation (Malles et al., 2023). The rapid grounding line depth change observed at Xeitl Sit' would have a large effect on reducing submarine melt rates and stabilizing iceberg calving. Consideration of decadal changes in subglacial topography that reduce terminus area by ~3% per year, as observed at Xeitl Sit', increases uncertainty in future projection of tidewater glacier evolution. Grounding line change also changes the depth at which the subglacial discharge plume intrudes into the fjord, potentially changing fjord mixing and heat transport to the terminus (Carroll et al., 2015, 2017; Hager et al., 2022). Glacier surface drawdown increases subglacial discharge volumes, increasing submarine melt, which is potentially limited by the buttressing force of the morainal bank (Amundson & Carroll, 2018).

CHAPTER V

CONCLUSION

Observations of bathymetric change in Xeitl Geeyí (LeConte Bay), Alaska provide insights into moraine building processes occurring during tidewater glacier fluctuations. Sediment accumulation rates are found to decrease exponentially with distance down-fjord, peaking at 6-20 m yr^{-1} at the glacier terminus and decreasing to 1-4 m yr^{-1}. Linear sediment accumulation rates increased over 25 years from 6-10 m yr^{-1} during 1999-2016 to 15-20 m yr^{-1} in 2018-2025. Xeitl Sit' may be at the beginning stages of a slow advance, facilitated by morainal bank growth. Increased sediment output may be caused by remobilization of previously deposited till, leading to increased moraine building stabilizing the glacier against climate-induced retreat. Glacier velocities are found to decelerate during moraine building and near terminus glacier elevation increases with increased moraine height. Observations of moraine building with glacier dynamics highlight the importance of modeling sediment dynamics when predicting the evolution of a tidewater glacier.

APPENDIX A. SUBGLACIAL DISCHARGE MODEL

To explore the relationship between sediment output and subglacial meltwater discharge, we run a Surface Mass Balance (SMB) model that incorporates an enhanced temperature index model and an accumulation model to calculate meltwater runoff (Hock, 1999; Hock & Noetzli, 1997). We employ a similar overall methodology to previous studies of Xeitl Sit' (e.g., Amundson et al., 2020, Jackson et al., 2022, Sutherland et al., 2019), but extend the time period to cover through summer 2025. Meltwater runoff is assumed to be transported instantaneously to the glacier's terminus and represents a terminus-averaged subglacial discharge value. We force the model with air temperature and hourly precipitation from the Petersburg Airport (PSG) weather station located 40 km from the glacier, adjusted for lapse rate using transfer functions (Eqns A-1, A-2). PSG climate data are downloaded from the Iowa State University Environmental Mesonet website (https://mesonet.agron.iastate.edu/request/download.phtml?network=AK_ASOS). To get error estimates, we vary model parameters to produce a high, moderate, and low melt scenario.

The following transfer functions are used to linearly scale Petersburg Airport weather data to that of the glacier's terminus 40 km away. $T_{glacier}$ and $P_{glacier}$ are the temperature and precipitation at the glacier's terminus, respectively and $T_{airport}$ and $P_{airport}$ are the temperature and precipitation at the airport, respectively. Transfer functions are established by comparing weather station data in 2016-2017 with overlapping airport weather data, creating a linear fit between the two (Jackson et al., 2020).

$$T_{glacier} = -1.5627\ ℃ + T_{airport} * 0.9649 \quad \text{(A-1)}$$

$$P_{glacier} = P_{airport} * 2.4583 \quad \text{(A-2)}$$

APPENDIX B. SUPPLEMENTAL FIGURES

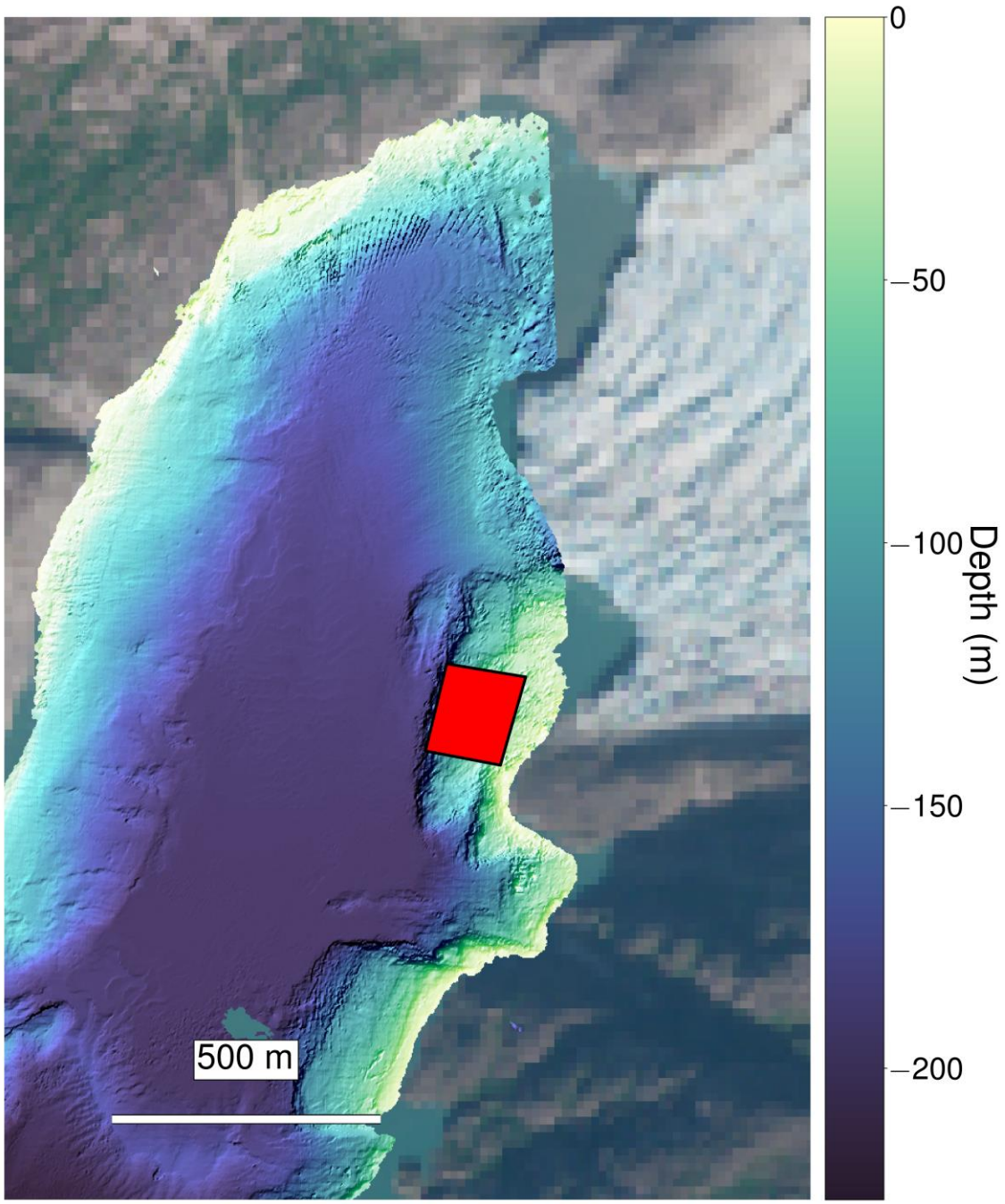


Figure A-1. Location of stable bedrock used for error estimation. Red highlighted region is used for error estimation of bathymetry. The average elevation change within the region for each set of years is calculated, and the largest elevation change is used as the bathymetry uncertainty.

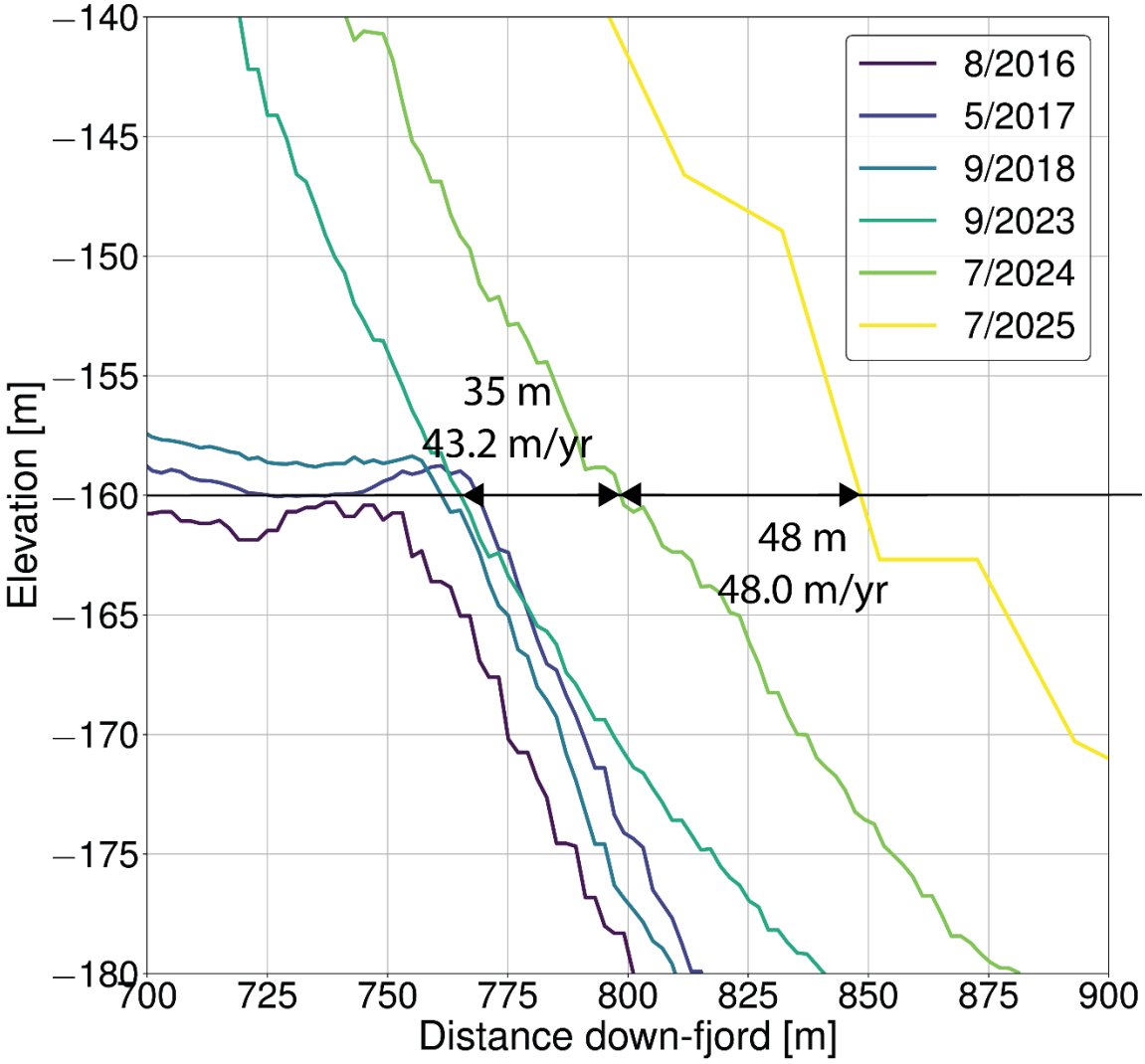


Figure A-2. Centerline elevation along the middle centerline shown in Figure 4d, zoomed in to -140 to -180 m depth. Dark bold line highlights moraine progradation at the -160 m isobath, and the annotated values are horizontal distance and rate of horizontal change.

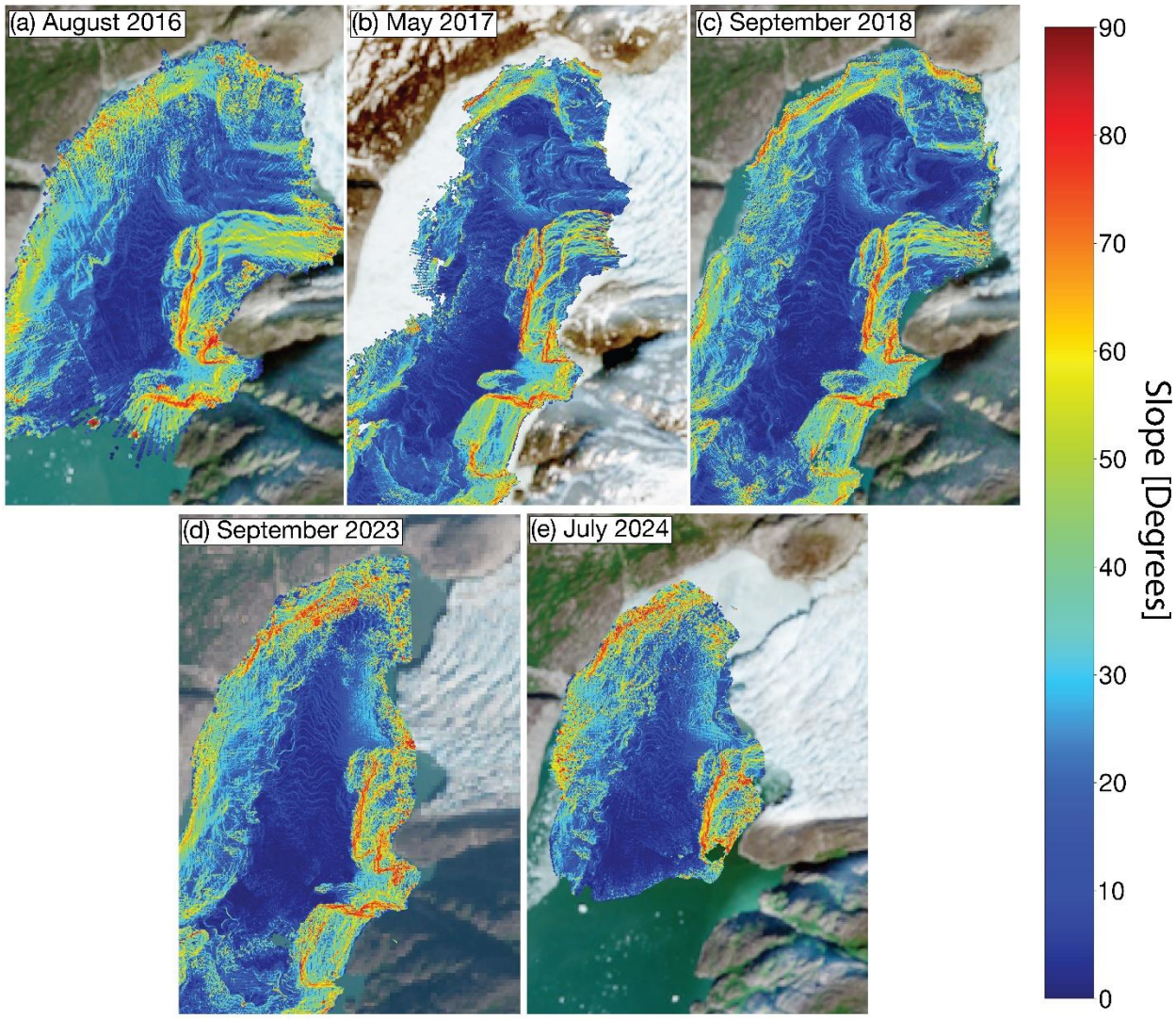


Figure A-3. Slope maps for (a) August 2016, (b) May 2017, (c) September 2018, (d) September 2023, (e) July 2024. Background imagery is from Sentinel-2.

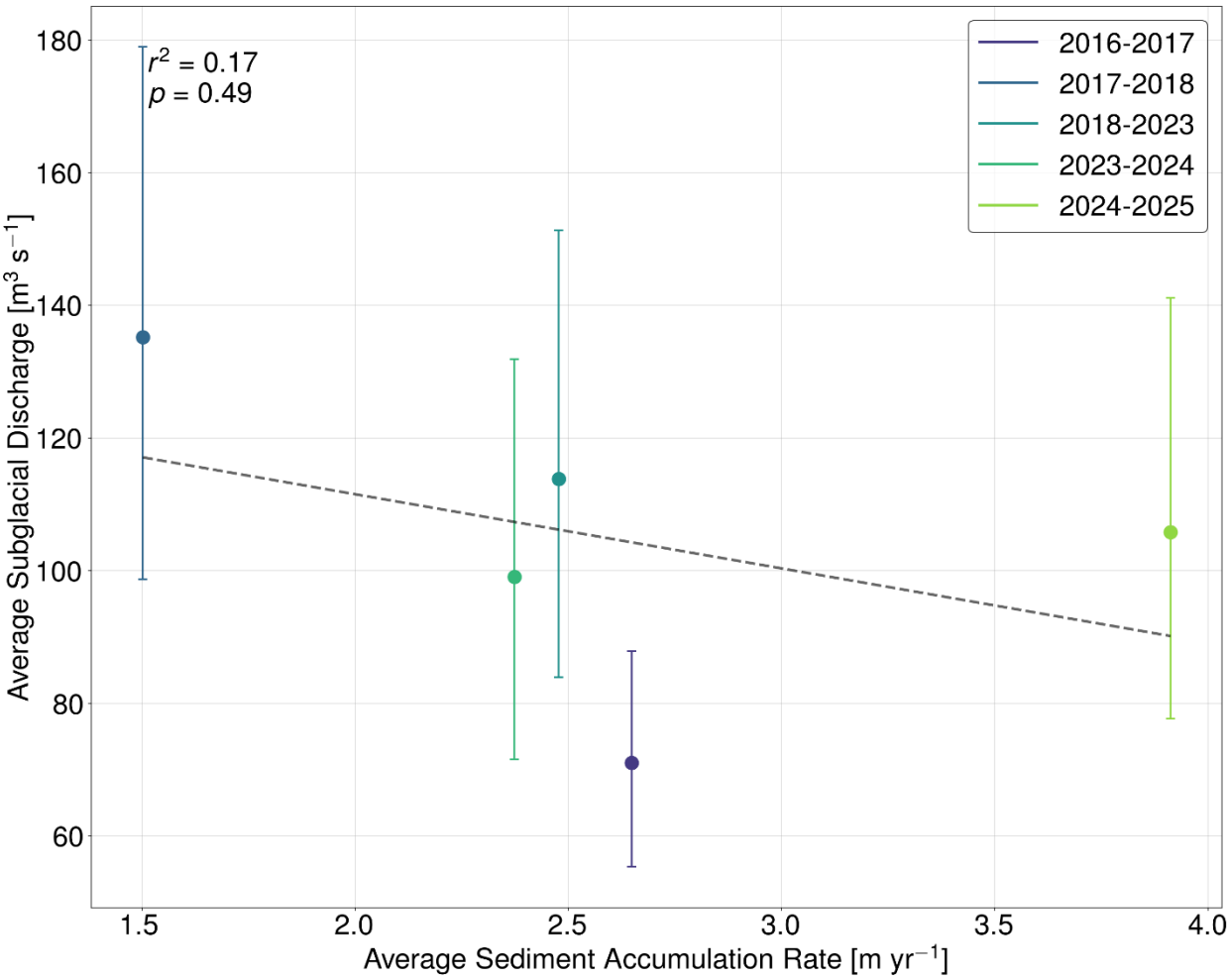


Figure A-4. Average summer subglacial discharge between field seasons plotted against average sediment accumulation rate in the basin downstream of the moraine. Dashed gray line is a line of best fit, with $r^2 = 0.17$ and $p = 0.49$.

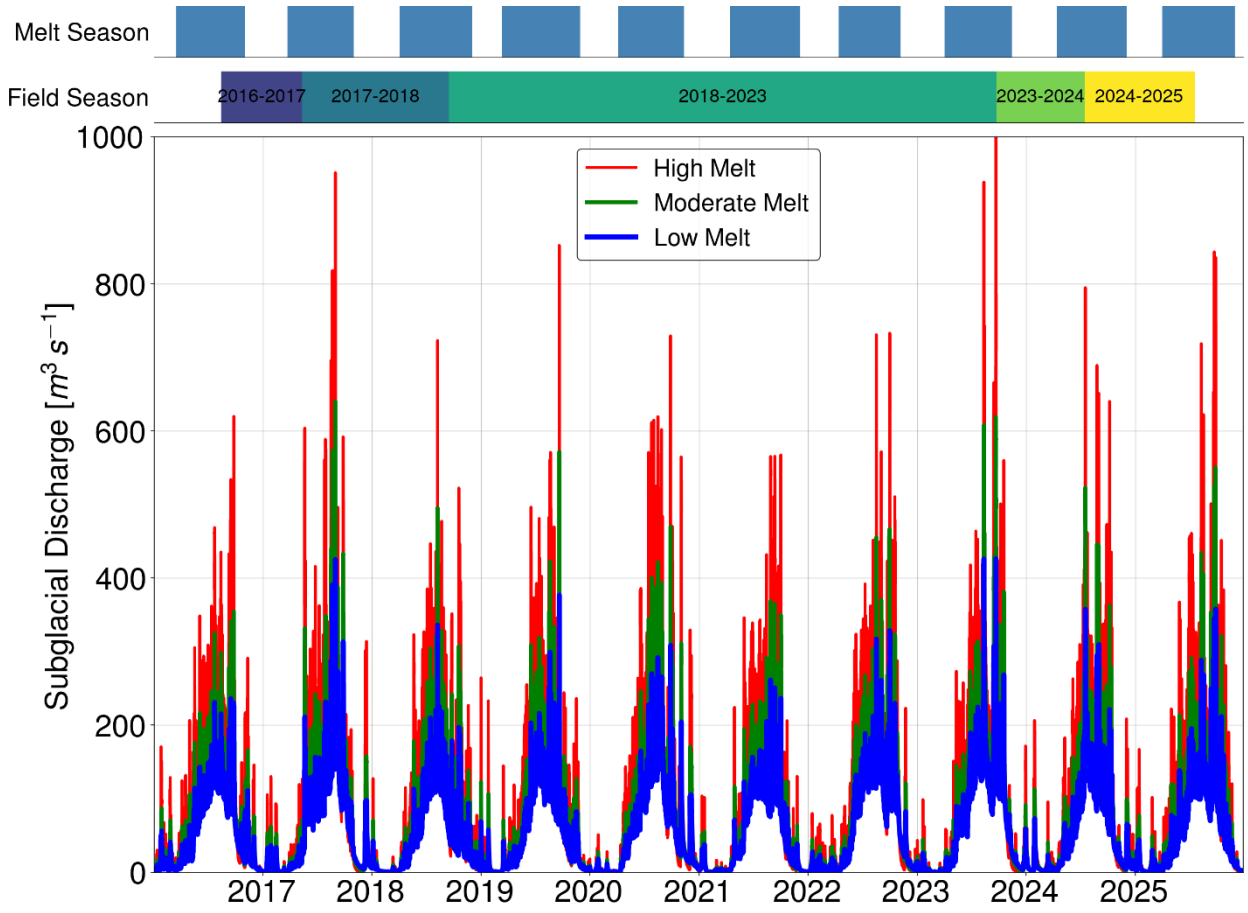


Figure A-5. Modeled subglacial discharge from 2016 to 2026 for a low, moderate, and high melt scenario. Summer melt seasons and field seasons are labeled above the main plot.

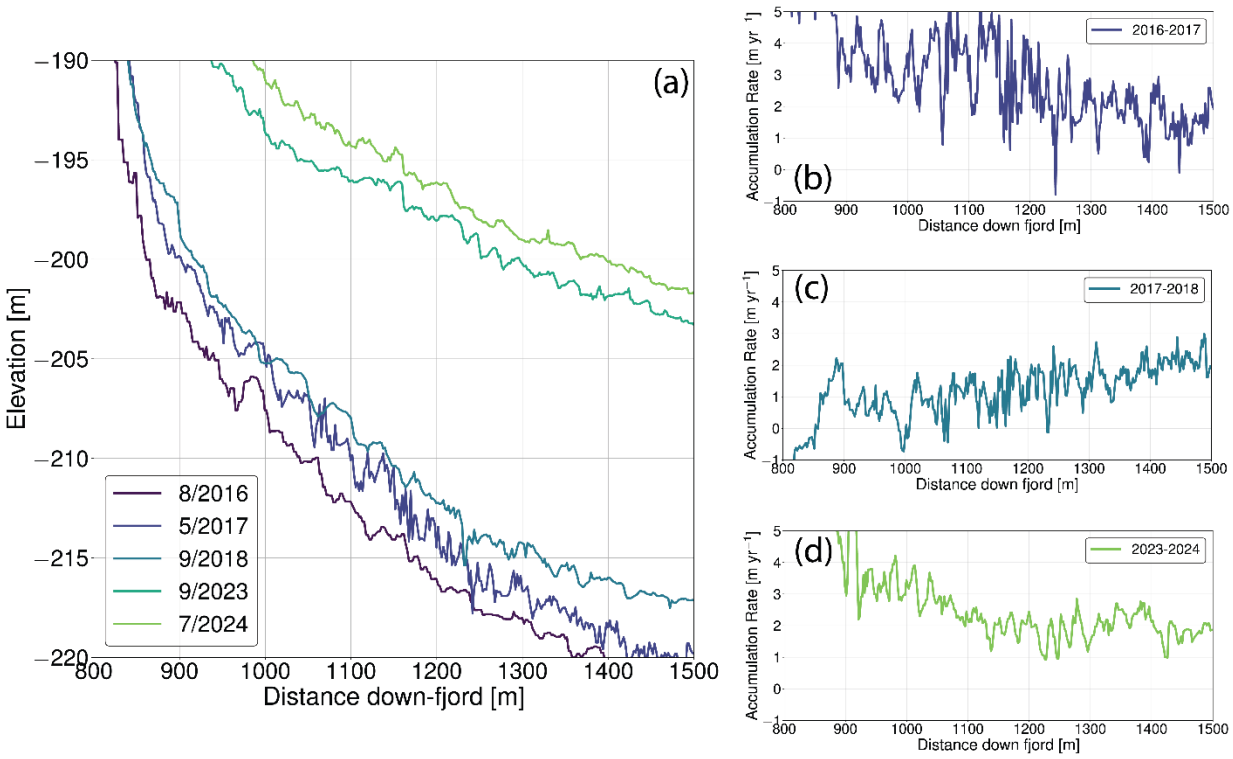


Figure A-6. (a) Centerline elevation along the middle centerline in Figure 4d, zoomed in to -190 to -220 m depth to highlight dune-like features. (b-d) Accumulation rates corresponding to the elevations shown in (a).

REFERENCES CITED

Abib, N., Sutherland, D. A., Amundson, J. M., Duncan, D., Eidam, E. F., Jackson, R. H., Kienholz, C., Morlighem, M., Motyka, R. J., Nash, J. D., Ovall, B., & Pettit, E. C. (2023). Persistent overcut regions dominate the terminus morphology of a rapidly melting tidewater glacier. *Annals of Glaciology*, *64*(90), 1–12. https://doi.org/10.1017/aog.2023.38

Alley, R. B., Cuffey, K. M., & Zoet, L. K. (2019). Glacial erosion: Status and outlook. *Annals of Glaciology*, *60*(80), 1–13. https://doi.org/10.1017/aog.2019.38

Amundson, J. M. (2016). A mass-flux perspective of the tidewater glacier cycle. *Journal of Glaciology*, *62*(231), 82–93. https://doi.org/10.1017/jog.2016.14

Amundson, J. M., & Carroll, D. (2018). Effect of Topography on Subglacial Discharge and Submarine Melting During Tidewater Glacier Retreat. *Journal of Geophysical Research: Earth Surface*, *123*(1), 66–79. https://doi.org/10.1002/2017JF004376

Amundson, J. M., Kienholz, C., Hager, A. O., Jackson, R. H., Motyka, R. J., Nash, J. D., & Sutherland, D. A. (2020). Formation, flow and break-up of ephemeral ice mélange at LeConte Glacier and Bay, Alaska. *Journal of Glaciology*, *66*(258), 577–590. https://doi.org/10.1017/jog.2020.29

Andresen, C. S., Karlsson, N. B., Straneo, F., Schmidt, S., Andersen, T. J., Eidam, E. F., Bjørk, A. A., Dartiguemalle, N., Dyke, L. M., Vermassen, F., & Gundel, I. E. (2024). Sediment discharge from Greenland's marine-terminating glaciers is linked with surface melt. *Nature Communications*, *15*(1), 1332. https://doi.org/10.1038/s41467-024-45694-1

Aschwanden, A., Bartholomaus, T. C., Brinkerhoff, D. J., & Truffer, M. (2021). Brief communication: A roadmap towards credible projections of ice sheet contribution to sea level. *The Cryosphere*, *15*(12), 5705–5715. https://doi.org/10.5194/tc-15-5705-2021

Barclay, D. J., Wiles, G. C., & Calkin, P. E. (2009). Holocene glacier fluctuations in Alaska. *Quaternary Science Reviews*, *28*(21–22), 2034–2048.

Barletta, V. R., Bevis, M., Smith, B. E., Wilson, T., Brown, A., Bordoni, A., Willis, M., Khan, S. A., Rovira-Navarro, M., Dalziel, I., Smalley, R., Kendrick, E., Konfal, S., Caccamise, D. J., Aster, R. C., Nyblade, A., & Wiens, D. A. (2018). Observed rapid bedrock uplift in Amundsen Sea Embayment promotes ice-sheet stability. *Science*, *360*(6395), 1335–1339. https://doi.org/10.1126/science.aao1447

Bartholomaus, T. C., Larsen, C. F., & O'Neel, S. (2013). Does calving matter? Evidence for significant submarine melt. *Earth and Planetary Science Letters*, *380*, 21–30. https://doi.org/10.1016/j.epsl.2013.08.014

Benn, D. I., & Evans, D. J. A. (2010). *Glaciers & glaciation* (2nd ed). Hodder education.

Berthier, E., Larsen, C., Durkin, W. J., Willis, M. J., & Pritchard, M. E. (2018). Brief communication: Unabated wastage of the Juneau and Stikine icefields (southeast Alaska) in the early 21st century. *The Cryosphere*, *12*(4), 1523–1530. https://doi.org/10.5194/tc-12-1523-2018

Boldt Love, K., Hallet, B., Pratt, T. L., & O'Neel, S. (2016). Observations and modeling of fjord sedimentation during the 30 year retreat of Columbia Glacier, AK. *Journal of Glaciology*, *62*(234), 778–793. https://doi.org/10.1017/jog.2016.67

Brew, D. A., & Friedman, R. M. (2000). *Notes on the Bedrock Geology and Geography of the Stikine Icefield, Coast Mountains Complex, Southeastern Alaska* (pp. 77–82) [Professional Paper]. U.S. Geological Survey.

Brinkerhoff, D., Truffer, M., & Aschwanden, A. (2017). Sediment transport drives tidewater glacier periodicity. *Nature Communications*, *8*(1), 90. https://doi.org/10.1038/s41467-017-00095-5

Caress, D. W., & Chayes, D. N. (1996). Improved processing of Hydrosweep DS multibeam data on the R/V Maurice Ewing. *Marine Geophysical Researches*, *18*(6), 631–650. https://doi.org/10.1007/BF00313878

Carroll, D., Sutherland, D. A., Shroyer, E. L., Nash, J. D., Catania, G. A., & Stearns, L. A. (2015). Modeling Turbulent Subglacial Meltwater Plumes: Implications for Fjord-Scale Buoyancy-Driven Circulation. *Journal of Physical Oceanography*, *45*(8), 2169–2185. https://doi.org/10.1175/JPO-D-15-0033.1

Carroll, D., Sutherland, D. A., Shroyer, E. L., Nash, J. D., Catania, G. A., & Stearns, L. A. (2017). Subglacial discharge-driven renewal of tidewater glacier fjords. *Journal of Geophysical Research: Oceans*, *122*(8), 6611–6629. https://doi.org/10.1002/2017JC012962

Catania, G. A., Stearns, L. A., Sutherland, D. A., Fried, M. J., Bartholomaus, T. C., Morlighem, M., Shroyer, E., & Nash, J. (2018). Geometric Controls on Tidewater Glacier Retreat in Central Western Greenland. *Journal of Geophysical Research: Earth Surface*, *123*(8), 2024–2038. https://doi.org/10.1029/2017JF004499

Cook, S. J., Swift, D. A., Kirkbride, M. P., Knight, P. G., & Waller, R. I. (2020). The empirical basis for modelling glacial erosion rates. *Nature Communications*, *11*(1), 759. https://doi.org/10.1038/s41467-020-14583-8

Cowan, E. A., & Powell, R. D. (1991). Ice-proximal sediment accumulation rates in a temperate glacial fjord, southeastern Alaska. *Geological Society of America Special Papers*. https://doi.org/10.1130/spe261-p61

Cowan, E. A., Seramur, K. C., Powell, R. D., Willems, B. A., & Et., A. (2010). Fjords as temporary sediment traps: History of glacial erosion and deposition in Muir Inlet, Glacier Bay National Park, southeastern Alaska. *Geological Society of America Bulletin*. https://doi.org/10.1130/b26595.1

Delaney, I., Anderson, L., & Herman, F. (2023). Modeling the spatially distributed nature of subglacial sediment transport and erosion. *Earth Surface Dynamics*, *11*(4), 663–680. https://doi.org/10.5194/esurf-11-663-2023

Derkacheva, A., Mouginot, J., Millan, R., Maier, N., & Gillet-Chaulet, F. (2020). Data Reduction Using Statistical and Regression Approaches for Ice Velocity Derived by Landsat-8, Sentinel-1 and Sentinel-2. *Remote Sensing*, *12*(12), 1935. https://doi.org/10.3390/rs12121935

Di Lorenzo, E., & Mantua, N. (2016). Multi-year persistence of the 2014/15 North Pacific marine heatwave. *Nature Climate Change*, *6*(11), 1042–1047. https://doi.org/10.1038/nclimate3082

Dowdeswell, J. A., Hogan, K. A., Arnold, N. S., Mugford, R. I., Wells, M., Hirst, J. P. P., & Decalf, C. (2015). Sediment-rich meltwater plumes and ice-proximal fans at the margins

of modern and ancient tidewater glaciers: Observations and modelling. *Sedimentology*, *62*(6), 1665–1692. https://doi.org/10.1111/sed.12198

Dühnforth, M., Anderson, R. S., Ward, D., & Stock, G. M. (2010). Bedrock fracture control of glacial erosion processes and rates. *Geology*, *38*(5), 423–426. https://doi.org/10.1130/G30576.1

Eidam, E. F., Nittrouer, C. A., Lundesgaard, Ø., Homolka, K. K., & Smith, C. R. (2019). Variability of Sediment Accumulation Rates in an Antarctic Fjord. *Geophysical Research Letters*, *46*(22), 13271–13280. https://doi.org/10.1029/2019GL084499

Eidam, E. F., Sutherland, D. A., Duncan, D., Kienholz, C., Amundson, J. M., & Motyka, R. J. (2020). Morainal Bank Evolution and Impact on Terminus Dynamics During a Tidewater Glacier Stillstand. *Journal of Geophysical Research: Earth Surface*, *125*(11), e2019JF005359. https://doi.org/10.1029/2019JF005359

Farr, T. G., Rosen, P. A., Caro, E., Crippen, R., Duren, R., Hensley, S., Kobrick, M., Paller, M., Rodriguez, E., Roth, L., Seal, D., Shaffer, S., Shimada, J., Umland, J., Werner, M., Oskin, M., Burbank, D., & Alsdorf, D. (2007). The Shuttle Radar Topography Mission. *Reviews of Geophysics*, *45*(2). https://doi.org/10.1029/2005RG000183

Fischer, E., & Aschwanden, A. (2024). Assessing the effects of fjord geometry on Greenland tidewater glacier stability. *Journal of Glaciology*, *70*, e53. https://doi.org/10.1017/jog.2024.55

Fischer, M. P., & Powell, R. D. (1998). A simple model for the influence of push-morainal banks on the calving and stability of glacial tidewater termini. *Journal of Glaciology*, *44*(146), 31–41. https://doi.org/10.3189/S002214300000232X

Gardner, A., Fahnestock, M., & Scambos, T. (2022). *MEaSUREs ITS_LIVE Regional Glacier and Ice Sheet Surface Velocities, Version 1*. NASA National Snow and Ice Data Center Distributed Active Archive Center. https://doi.org/10.5067/6II6VW8LLWJ7

Gardner, A., Moholdt, G., Scambos, T., Fahnstock, M., Ligtenberg, S., van den Broeke, M., & Nilsson, J. (2018). Increased West Antarctic and unchanged East Antarctic ice discharge over the last 7 years. *The Cryosphere*, *12*(2), 521–547. https://doi.org/10.5194/tc-12-521-2018

Goff, J. A., Lawson, D. E., Willems, B. A., Davis, M., & Gulick, S. P. S. (2012). Morainal bank progradation and sediment accumulation in Disenchantment Bay, Alaska: Response to advancing Hubbard Glacier. *Journal of Geophysical Research: Earth Surface*, *117*(F2), 2011JF002312. https://doi.org/10.1029/2011JF002312

Hager, A. O., Sutherland, D. A., Amundson, J. M., Jackson, R. H., Kienholz, C., Motyka, R. J., & Nash, J. D. (2022). Subglacial Discharge Reflux and Buoyancy Forcing Drive Seasonality in a Silled Glacial Fjord. *Journal of Geophysical Research: Oceans*, *127*(5), e2021JC018355. https://doi.org/10.1029/2021JC018355

Hallet, B., Hunter, L., & Bogen, J. (1996). Rates of erosion and sediment evacuation by glaciers: A review of field data and their implications. *Global and Planetary Change*. https://doi.org/10.1016/0921-8181(95)00021-6

Herman, F., Beyssac, O., Brughelli, M., Lane, S. N., Leprince, S., Adatte, T., Lin, J. Y. Y., Avouac, J.-P., & Cox, S. C. (2015). Erosion by an Alpine glacier. *Science*, *350*(6257), 193–195. https://doi.org/10.1126/science.aab2386

Herman, F., De Doncker, F., Delaney, I., Prasicek, G., & Koppes, M. (2021). The impact of glaciers on mountain erosion. *Nature Reviews Earth & Environment*, *2*(6), 422–435. https://doi.org/10.1038/s43017-021-00165-9

Hewitt, I. J. (2020). Subglacial Plumes. *Annual Review of Fluid Mechanics*, *52*(1), 145–169. https://doi.org/10.1146/annurev-fluid-010719-060252

Hock, R. (1999). A distributed temperature-index ice- and snowmelt model including potential direct solar radiation. *Journal of Glaciology*, *45*(149), 101–111. https://doi.org/10.3189/S0022143000003087

Hock, R., & Noetzli, C. (1997). Areal melt and discharge modelling of Storglaciären, Sweden. *Annals of Glaciology*, *24*, 211–216. https://doi.org/https://doi.org/10.3189/S0260305500012192

Hoek, E., & Bray, J. D. (1981). *Rock slope engineering*. CRC press.

Hooyer, T. S., Cohen, D., & Iverson, N. R. (2012). Control of glacial quarrying by bedrock joints. *Geomorphology*, *153–154*, 91–101. https://doi.org/10.1016/j.geomorph.2012.02.012

Hunter, L. E., & Powell, R. D. (1995). Effects of ice-proximal sediment dynamics on the stability of Muir Glacier, Glacier Bay, Alaska. *Proceedings of the Third Glacier Bay Science Symposium, Edited by D. Engstrom*, 29–37.

Hunter, L. E., Powell, R. D., & Lawson, D. E. (1996). Morainal-bank sediment budgets and their influence on the stability of tidewater termini of valley glaciers entering Glacier Bay, Alaska, U.S.A. *Annals of Glaciology*, *22*, 211–216. https://doi.org/10.3189/1996AoG22-1-211-216

Jackson, R. H., Motyka, R. J., Amundson, J. M., Abib, N., Sutherland, D. A., Nash, J. D., & Kienholz, C. (2022). The Relationship Between Submarine Melt and Subglacial Discharge From Observations at a Tidewater Glacier. *Journal of Geophysical Research: Oceans*, *127*(10), e2021JC018204. https://doi.org/10.1029/2021JC018204

Jackson, R. H., Nash, J. D., Kienholz, C., Sutherland, D. A., Amundson, J. M., Motyka, R. J., Winters, D., Skyllingstad, E., & Pettit, E. C. (2020). Meltwater Intrusions Reveal Mechanisms for Rapid Submarine Melt at a Tidewater Glacier. *Geophysical Research Letters*, *47*(2), e2019GL085335. https://doi.org/10.1029/2019GL085335

Kaluzienski, L. M., Amundson, J. M., Womble, J. N., Bliss, A. K., & Pearson, L. E. (2023). Impacts of tidewater glacier advance on iceberg habitat. *Annals of Glaciology*, *64*(90), 44–54. https://doi.org/10.1017/aog.2023.46

Kehrl, L. M., Hawley, R. L., Powell, R. D., & Brigham-Grette, J. (2011). Glacimarine sedimentation processes at Kronebreen and Kongsvegen, Svalbard. *Journal of Glaciology*, *57*(205), 841–847. https://doi.org/10.3189/002214311798043708

Koppes, M., Hallet, B., Rignot, E., Mouginot, J., Wellner, J. S., & Boldt, K. (2015). Observed latitudinal variations in erosion as a function of glacier dynamics. *Nature*, *526*(7571), 100–103. https://doi.org/10.1038/nature15385

Krabbendam, M., & Glasser, N. F. (2011). Glacial erosion and bedrock properties in NW Scotland: Abrasion and plucking, hardness and joint spacing. *Geomorphology*, *130*(3), 374–383. https://doi.org/10.1016/j.geomorph.2011.04.022

Larter, R. D., & Barker, P. F. (1989). Seismic stratigraphy of the Antarctic Peninsula Pacific margin: A record of Pliocene-Pleistocene ice volume and paleoclimate. *Geology*, *17*(8), 731–734.

Lea, J. M. (2018). The Google Earth Engine Digitisation Tool (GEEDiT) and the Margin change Quantification Tool (MaQiT) – simple tools for the rapid mapping and quantification of changing Earth surface margins. *Earth Surface Dynamics*, *6*(3), 551–561. https://doi.org/10.5194/esurf-6-551-2018

Malles, J.-H., Maussion, F., Ultee, L., Kochtitzky, W., Copland, L., & Marzeion, B. (2023). Exploring the impact of a frontal ablation parameterization on projected 21st-century mass change for Northern Hemisphere glaciers. *Journal of Glaciology*, *69*(277), 1317–1332. https://doi.org/10.1017/jog.2023.19

McConnochie, C. D., & Cenedese, C. (2023). Increased Melting of Marine-Terminating Glaciers by Sediment-Laden Plumes. *Geophysical Research Letters*, *50*(20), e2023GL103736. https://doi.org/10.1029/2023GL103736

Meier, M. F., & Post, A. (1987). Fast tidewater glaciers. *Journal of Geophysical Research: Solid Earth*, *92*(B9), 9051–9058. https://doi.org/10.1029/JB092iB09p09051

Melkonian, A. K., Willis, M. J., & Pritchard, M. E. (2016). Stikine Icefield Mass Loss between 2000 and 2013/2014. *Frontiers in Earth Science*, *4*. https://doi.org/10.3389/feart.2016.00089

Minowa, M., Skvarca, P., Fujita, K., Naito, N., & Sugiyama, S. (2026). Triggering mechanisms of dynamic mass loss at a freshwater-calving glacier in southern Patagonia. *Earth and Planetary Science Letters*, *681*, 119930. https://doi.org/10.1016/j.epsl.2026.119930

Motyka, R. J., & Begét, J. E. (1996). Taku Glacier, Southeast Alaska, U.S.A.: Late Holocene History of a Tidewater Glacier. *Arctic and Alpine Research*, *28*(1), 42–51. https://doi.org/10.2307/1552084

Motyka, R. J., Beget, J. E., & Bowen, P. (1998). *Recent retreat of LeConte Glacier and associated calving and iceberg hazards* (RI 98-15; p. RI 98-15). Alaska Division of Geological & Geophysical Surveys. https://doi.org/10.14509/2590

Motyka, R. J., Hunter, L., Echelmeyer, K. A., & Connor, C. (2003). Submarine melting at the terminus of a temperate tidewater glacier, LeConte Glacier, Alaska, U.S.A. *Annals of Glaciology*, *36*, 57–65. https://doi.org/10.3189/172756403781816374

Motyka, R. J., & Truffer, M. (2007). Hubbard Glacier, Alaska: 2002 closure and outburst of Russell Fjord and postflood conditions at Gilbert Point. *Journal of Geophysical Research: Earth Surface*, *112*(F2). https://doi.org/10.1029/2006JF000475

Motyka, R. J., Truffer, M., Kuriger, E. M., & Bucki, A. K. (2006). Rapid erosion of soft sediments by tidewater glacier advance: Taku Glacier, Alaska, USA. *Geophysical Research Letters*, *33*(24), 2006GL028467. https://doi.org/10.1029/2006GL028467

Mugford, R. I., & Dowdeswell, J. A. (2011). Modeling glacial meltwater plume dynamics and sedimentation in high-latitude fjords. *Journal of Geophysical Research: Earth Surface*, *116*(F1). https://doi.org/10.1029/2010JF001735

Norris, S. L., Gosse, J. C., Millan, R., Mouginot, J., Rabatel, A., Morlighem, M., Bolton, M. S. M., & Alley, R. B. (2025). Drivers of global glacial erosion rates. *Nature Geoscience*, *18*(8), 732–739. https://doi.org/10.1038/s41561-025-01747-8

Nuth, C., & Kääb, A. (2011). Co-registration and bias corrections of satellite elevation data sets for quantifying glacier thickness change. *The Cryosphere*, *5*(1), 271–290. https://doi.org/10.5194/tc-5-271-2011

O'Neel, S., Echelmeyer, K. A., & Motyka, R. J. (2003). Short-term variations in calving of a tidewater glacier: LeConte Glacier, Alaska, U.S.A. *Journal of Glaciology*, *49*(167), 587–598. https://doi.org/10.3189/172756503781830430

O'Neel, S., Pfeffer, W. T., Krimmel, R., & Meier, M. (2005). Evolving force balance at Columbia Glacier, Alaska, during its rapid retreat. *Journal of Geophysical Research: Earth Surface*, *110*(F3). https://doi.org/10.1029/2005JF000292

Pierce, E., Overeem, I., & Hasholt, B. (2026). Sediment transport by Greenland's icebergs. *Nature Communications*, *17*(1), 1172. https://doi.org/10.1038/s41467-025-67938-4

Pope, E. L., Normandeau, A., Ó Cofaigh, C., Stokes, C. R., & Talling, P. J. (2019). Controls on the formation of turbidity current channels associated with marine-terminating glaciers and ice sheets. *Marine Geology*, *415*, 105951. https://doi.org/10.1016/j.margeo.2019.05.010

Porter, C., Morin, P., Howat, I., Noh, M.-J., Bates, B., Peterman, K., Keesey, S., Schlenk, M., Gardiner, J., & Tomko, K. (2018). ArcticDEM, version 3. *Harvard Dataverse Dataset*, 277.

Post, A., O'Neel, S., Motyka, R. J., & Streveler, G. (2011). A complex relationship between calving glaciers and climate. *Eos, Transactions American Geophysical Union*, *92*(37), 305–306. https://doi.org/10.1029/2011EO370001

RGI Consortium. (2023). *Randolph Glacier Inventory—A Dataset of Global Glacier Outlines, Version 7*. NASA National Snow and Ice Data Center Distributed Active Archive Center. https://doi.org/10.5067/F6JMOVY5NAVZ

Schimel, A. C. G., Ierodiaconou, D., Hulands, L., & Kennedy, D. M. (2015). Accounting for uncertainty in volumes of seabed change measured with repeat multibeam sonar surveys. *Continental Shelf Research*, *111*, 52–68. https://doi.org/10.1016/j.csr.2015.10.019

Schoof, C. (2007). Ice sheet grounding line dynamics: Steady states, stability, and hysteresis. *Journal of Geophysical Research: Earth Surface*, *112*(F3). https://doi.org/10.1029/2006JF000664

Seramur, K. C., Powell, R. D., & Carlson, P. R. (1997). Evaluation of conditions along the grounding line of temperate marine glaciers: An example from Muir Inlet, Glacier Bay, Alaska. *Marine Geology*, *140*(3–4), 307–327. https://doi.org/10.1016/S0025-3227(97)00026-1

Sergienko, O., Haseloff, M., Robel, A., & Wingham, D. (2026). A new paradigm for understanding Earth's marine ice sheets. *Nature Geoscience*. https://doi.org/10.1038/s41561-026-01941-2

Shionalyn, K., Catania, G., Trugman, D. T., Shahin, M. G., Stearns, L. A., & Felikson, D. (2026). Outlet glacier seasonal terminus prediction using interpretable machine learning. *The Cryosphere*, *20*(3), 1725–1744. https://doi.org/10.5194/tc-20-1725-2026

Slootman, A., & Cartigny, M. J. (2020). Cyclic steps: Review and aggradation-based classification. *Earth-Science Reviews*, *201*, 102949.

Stott, T., & Mount, N. (2007). Alpine proglacial suspended sediment dynamics in warm and cool ablation seasons: Implications for global warming. *Journal of Hydrology*. https://doi.org/10.1016/j.jhydrol.2006.07.001

Straneo, F., & Cenedese, C. (2015). The Dynamics of Greenland's Glacial Fjords and Their Role in Climate. *Annual Review of Marine Science*, *7*(1), 89–112. https://doi.org/10.1146/annurev-marine-010213-135133

Sutherland, D. A., Jackson, R. H., Kienholz, C., Amundson, J. M., Dryer, W. P., Duncan, D., Eidam, E. F., Motyka, R. J., & Nash, J. D. (2019). Direct observations of submarine melt and subsurface geometry at a tidewater glacier. *Science*, *365*(6451), 369–374. https://doi.org/10.1126/science.aax3528

Swift, D. A., Nienow, P. W., & Hoey, T. B. (2005). Basal sediment evacuation by subglacial meltwater: Suspended sediment transport from Haut Glacier d'Arolla, Switzerland. *Earth Surface Processes and Landforms*, *30*(7), 867–883. https://doi.org/10.1002/esp.1197

Truffer, M., Motyka, R. J., Hekkers, M., Howat, I. M., & King, M. A. (2009). Terminus dynamics at an advancing glacier: Taku Glacier, Alaska. *Journal of Glaciology*, *55*(194), 1052–1060. https://doi.org/10.3189/002214309790794887

Trusel, L. D., Powell, R. D., Cumpston, R. M., & Brigham-Grette, J. (2010). Modern glacimarine processes and potential future behaviour of Kronebreen and Kongsvegen polythermal tidewater glaciers, Kongsfjorden, Svalbard. *Geological Society, London, Special Publications*. https://doi.org/10.1144/sp344.9

xdem contributors. (2026). *xDEM* [Computer software]. Zenodo. https://doi.org/10.5281/zenodo.19636034

Zechmann, J. M., Truffer, M., Motyka, R. J., Amundson, J. M., & Larsen, C. F. (2021). Sediment redistribution beneath the terminus of an advancing glacier, Taku Glacier (T'aakú Kwáan Sít'i), Alaska. *Journal of Glaciology*, *67*(262), 204–218. https://doi.org/10.1017/jog.2020.101

Zeller, L., McGrath, D., Sass, L., Florentine, C., & Downs, J. (2025). Equilibrium line altitudes, accumulation areas and the vulnerability of glaciers in Alaska. *Journal of Glaciology*, *71*, e28. https://doi.org/10.1017/jog.2024.65